



Three-dimensional numerical models of flat slab subduction and the Denali fault driving deformation in south-central Alaska

Margarete A. Jadamec ^{a,*}, Magali I. Billen ^b, Sarah M. Roeske ^b

^a Department of Geological Sciences, Brown University, 324 Brook Street, Providence, RI 02912, United States

^b Department of Geology, University of California–Davis, One Shields Avenue, Davis, CA 95616, United States



ARTICLE INFO

Article history:

Received 21 November 2012

Received in revised form 11 May 2013

Accepted 8 June 2013

Available online 15 July 2013

Editor: Y. Ricard

Keywords:

flat slab subduction

lithosphere deformation

intra-continental faults

numerical models

Alaska

geodynamics

ABSTRACT

Early theories of plate tectonics assumed plates were rigid with deformation limited to within a few tens of kilometers of the plate boundary. However, observations indicate most continental plates defy such rigid behavior with deformation extending over 1000 kilometers inboard. We construct three-dimensional (3D) numerical models of the boundary between the Pacific and North American plates in Alaska to investigate the relative controls of flat slab subduction, continental scale faulting, and a non-linear rheology on deformation in the overriding plate. The models incorporate a realistic slab shape based on seismicity and seismic tomography and a variable thermal structure for both the subducting and overriding plates based on geologic and geophysical observables. The inclusion of the Denali fault in the models allows for the portion of south-central Alaska between the Denali fault and the trench to partially decouple from the rest of North America, forming an independently moving region that correlates to what has been described from geologic and geodetic studies as the Wrangell block. The motion of the Wrangell block tracks the motion of the flat slab in the subsurface indicating the subducting plate is driving the motion of the Wrangell block. Models using a composite (Newtonian and non-Newtonian) viscosity predict compressional motion along the northern bend in the Denali fault, consistent with thermochronologic data that show significant late Neogene exhumation in the central Alaska Range, including at Mt. McKinley, the tallest mountain in North America. These 3D numerical models of the Pacific–North American margin in Alaska show the subducting slab is the main driver of overriding plate deformation in south-central Alaska and combined with the Denali fault can reproduce several first order tectonic features of the region including the motion of the Wrangell block, uplift in the central Alaska Range, subsidence in the Cook Inlet–Susitna Basins, and upwelling at the slab edge beneath the Wrangell volcanics.

© 2013 The Authors. Published by Elsevier B.V. Open access under CC BY-NC-SA license.

1. Introduction

The theory of plate tectonics has changed from a paradigm focused on rigid plates, predicting deformation is limited to within a few tens of kilometers of the boundary, to a framework that allows for broad deformation zones extending over 1000 km inboard (Forsyth and Uyeda, 1975; England and Houseman, 1985; Molnar, 1988; Coleman and Hodges, 1995; Bird, 2003; Kreemer et al., 2003; Cook and Royden, 2008; Ghosh and Holt, 2012). With this comes the recognition that plate margins are inherently three-dimensional (3D) tectonic features, characterized by lateral variations in physical properties in both the subducting and overriding plates that may contribute to the observed deformation. For example the geophysical properties and morphology of a sub-

ducting plate can vary significantly within a subduction zone, including localized flat slab subduction as in the South American, Japan, and eastern Alaska subduction zones (Gudmundsson and Sambridge, 1998; Gutscher et al., 2000; Song and Simons, 2003; Lallemand et al., 2005; Martinod et al., 2005; Morra et al., 2006; Syracuse and Abbers, 2006; Müller et al., 2008). In addition, the overriding plate lithospheric structure often contains spatial heterogeneity including major intra-continental shear zones, such as the Altyn Tagh fault, the North Anatolian fault, and Denali fault, with these features commonly associated with oblique convergence and lateral extrusion of the overriding plate (England and Molnar, 1990; Avouac and Tapponnier, 1993; Yin et al., 2002; Redfield et al., 2007; Thatcher, 2009).

The Pacific–North America plate boundary in Alaska is a classic example of an inherently three-dimensional plate boundary with variations in subducting and overriding plate structure that may be significant in controlling the widespread deformation in the

* Corresponding author. Tel.: +1 773 332 0044; fax: +1 401 863 2058.

E-mail address: Margarete.Jadamec@Brown.edu (M.A. Jadamec).

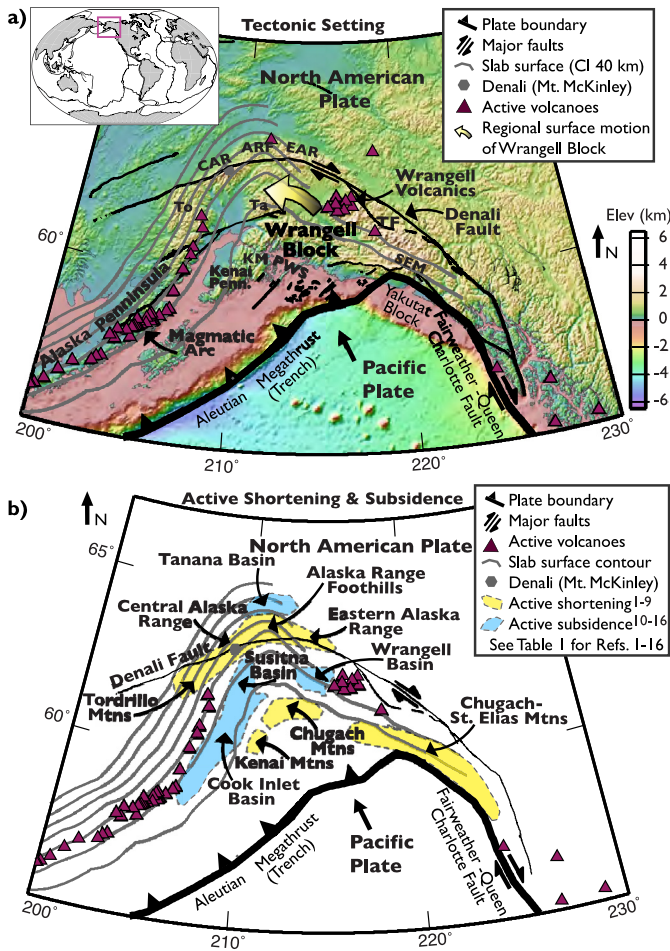


Fig. 1. Tectonic setting and locations of active shortening and subsidence in south-central Alaska. (a) Major faults (Plafker et al., 1994a), Holocene volcanoes (<http://www.avo.alaska.edu/>), and schematic arrow showing observed sense of motion of Wrangell block from GPS (Freymueller et al., 2008) superimposed on topography and bathymetry (Smith and Sandwell, 1997). Contours (gray) of slab surface show flat slab beneath south-central Alaska (Jadamec and Billen, 2010, 2012 and references therein. See also Section 2.1.2). (b) Locations of active shortening and subsidence (Table 1). ARF – Alaska Range Foothills, CAR – Central Alaska Range, EAR – Eastern Alaska Range, KM – Kenai Mountains, PWS – Prince William Sound, SEM – St. Elias Mountains, Ta – Talkeetna Mountains, TF – Totschunda Fault, To – Tordrillo Mountains.

overriding plate (Fig. 1). In the eastern part of the subduction zone, the northeast-trending Aleutian megathrust terminates against the northwest-trending Queen Charlotte–Fairweather transform fault forming a corner shaped subduction-transform plate boundary in map view (Plafker et al., 1994a, 1994b) (Fig. 1a). Seismic data and previous geodynamic modeling suggest the form of the subducting plate is that of a flat slab containing a two-tiered slab edge (Page et al., 1989; Fuis et al., 2008; Ratchkovski and Hansen, 2002; Eberhart-Phillips et al., 2006; Jadamec and Billen, 2010, 2012). In the plate boundary corner, the location of the flat slab coincides with abnormally thick mafic crust interpreted to be a subducted oceanic plateau, referred to as the Yakutat block (Brocher et al., 1994; Ferris et al., 2003; Eberhart-Phillips et al., 2006; Fuis et al., 2008).

The overriding North American plate in Alaska is characterized by a history of terrane accretion and major intra-continental faulting (Nokleberg et al., 1994). The Denali fault is a long lived arcuate shaped strike-slip fault inboard of the plate boundary that currently accommodates significant motion as indicated by the recent 7.9 Mw earthquake (Stout and Chase, 1980; Plafker et al., 1994a; Eberhart-Phillips et al., 2003) (Fig. 1). The fault has accommo-

Table 1
Summary of young exhumation and subsidence in south-central Alaska.

Areas of exhumation	Elev. (km)	Youngest Exh. Age (Ma)	Isotopic system
Denali (Mt. McKinley) ^{1,2}	6.2	5–6	AFT
Central Alaska Range ^{2*}	1–6.2	5–6	AFT
Eastern Alaska Range ³	1.5–4	1–10	K-feldspar 40Ar/39Ar AFT, AHe
Tordrillo Mountains ^{4,5}	1.5–2.5	6–7	AFT
W. Chugach Mtns ⁶	0–4	4–10	AFT, AHe
E. Chugach Mtns N ^{7,8}	1–2.5	5–10	AFT, AHe
E. Chugach Mtns S ^{7,8}	0–3	0.4–10	ZFT, AFT, AHe
St. Elias Mtns ^{7,9}	1.5–5	0.5–10	ZFT, AFT, AHe

Areas of subsidence	Thickn. (km)	Time span
Cook Inlet Basin ^{10,11}	~ 3	Mioc.-Quat.
Susitna Basin ¹²	≤ 3.5	Tert.
Wrangell Basin ¹³	≤ 1.0	Tert.
Tanana Basin ^{14,15,16}	~ 2	Mioc.-Quat.

Elev. – modern topographic elevation. Exh. age – exhumation age from studies listed. Thickn. – Sedimentary thickness from studies listed.

^{1,2}Fitzgerald et al. (1993, 1995); ^{2*}Central Alaska Range values extrapolated from Figures 10 and 11 in Fitzgerald et al. (1995); ³Benowitz et al. (2011), ⁴Haeussler (2008); ⁵Benowitz et al. (2012); ⁶Arkle et al. (2013); ⁷Spotila et al. (2004); ⁸Ferguson et al. (2012); ⁹Enkelmann et al. (2009); ¹⁰Hartman et al. (1974); ¹¹Dallegge and Layer (2004); ¹²Meyer and Boggess (2003a); ¹³Meyer and Boggess (2003b); ¹⁴Wahrhaftig (1987); ¹⁵Triplehorn et al. (2000); ¹⁶Ridgway et al. (2007). Location of active shortening in Alaska Range foothills from Bemis and Wallace (2007) and Bemis et al. (2012) is shown in Fig. 1, although the magnitude is not quantified here.

AFT – Apatite Fission-Track, AHe – Apatite–Helium, ZFT – Zircon Fission-Track.

dated 100s of km of displacement since its inception in the Cretaceous (Stout and Chase, 1980; Plafker et al., 1994a). The sense of slip is predominantly right-lateral, although splays off the Denali fault indicate thrust faulting and active convergence associated with the northern bend of the fault (Plafker et al., 1994a; Bemis and Wallace, 2007; Haeussler, 2008; Bemis et al., 2012).

As expected by 2D thin sheet models of viscous deformation (England et al., 1985), active mountain building and exhumation occur adjacent to the plate boundary in the Chugach–St. Elias mountains (Bruhn et al., 2004; Enkelmann et al., 2009) (Fig. 1b and Table 1). However, young exhumation also occurs approximately 500 km inboard of the plate margin in the central (Fitzgerald et al., 1993, 1995) and eastern (Benowitz et al., 2011) Alaska ranges, located along the northern arc in the Denali fault (Fig. 1b and Table 1).

Which tectonic components are most significant in controlling deformation in the overriding plate remains an outstanding question at broad plate boundaries. For example, in Alaska, is it the flat slab subduction, lithosphere-scale faults in the overriding plate, lateral strength variations in the overriding plate due to a history of terrane accretion, the ongoing collision of the Yakutat block, or factors external to mainland Alaska such as a change in Pacific plate motion or differential motion between the North American and Eurasian plates (Schultz and Aydin, 1990; Fitzgerald et al., 1993; Plafker et al., 1994a, 1994b; Bird, 1996; Redfield et al., 2007; Haeussler, 2008; Freymueller et al., 2008; Jadamec and Billen, 2010; Finzel et al., 2011)?

There are very few 3D geodynamic models of the Alaska plate boundary that test for the competing effects of the subducting and overriding plate by including an actual slab as well as upper plate (Jadamec, 2009; Jadamec and Billen, 2010, 2012; Ali and Freed, 2010; Jadamec and Billen, 2012). For example, the majority of models are either kinematic models or dynamic models which are kinematically driven, prescribe basal tractions to the litho-

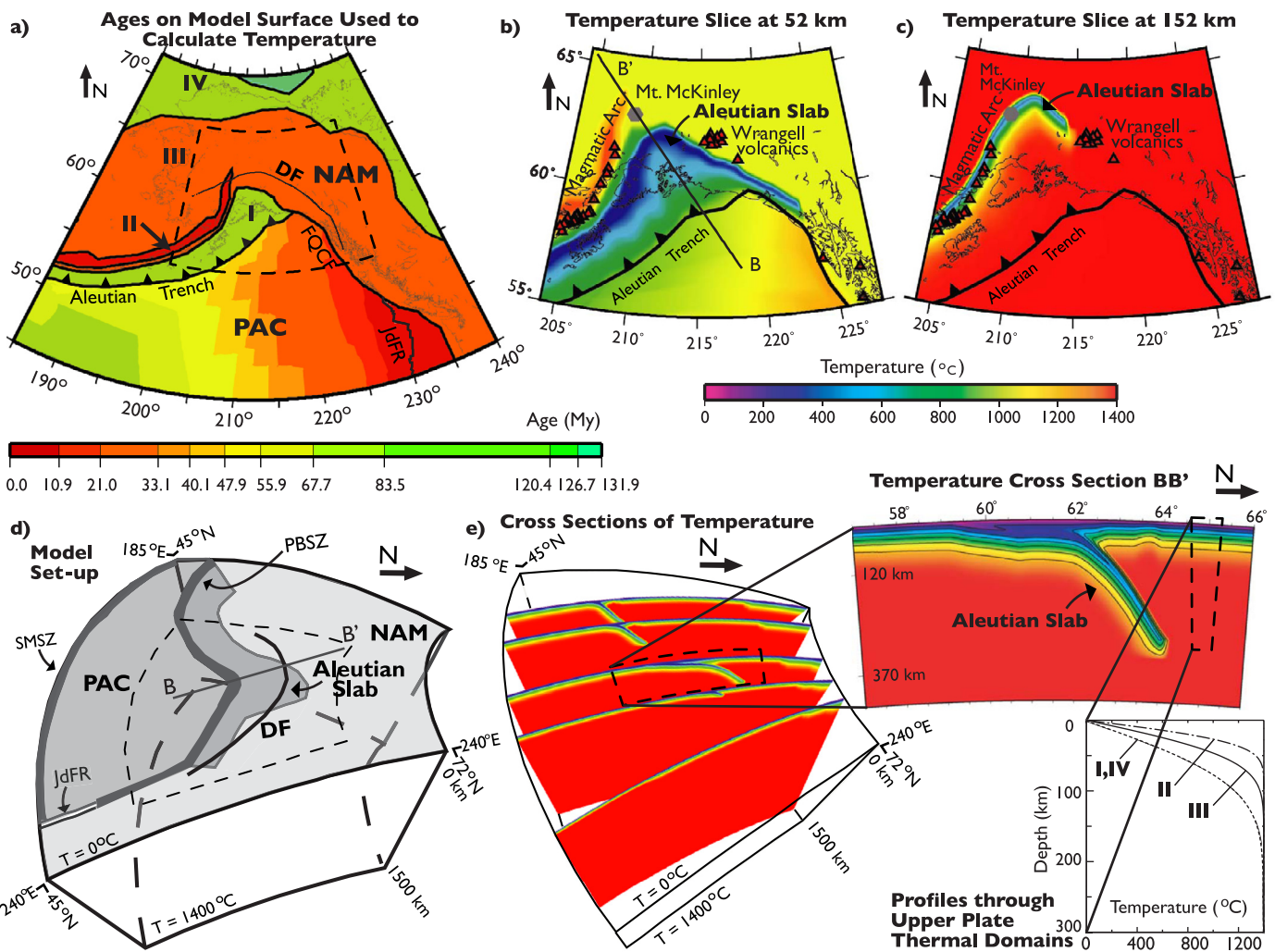


Fig. 2. Three-dimensional thermal structure and model domain used in geodynamic model. (a) Ages on model surface used to calculate lithospheric temperature. Seafloor ages from Müller et al. (1997). Overriding plate effective ages from integrated data (see Section 2.1.2), with the following thermal domains: I – forearc, II – magmatic arc, III – Cordillera, IV – Ancestral North America. (b), (c) Radial slices through model temperature at 52 km and 152 km for dashed region in (a). (d) Cartoon of model domain and set-up used in finite-element model. (e) Cross sections through model temperature show along strike variation in slab dip and temperature. Inset shows temperature cross section BB' and profiles of upper plate thermal domains. Longitude and latitude range of plot in (a) shows full model bounds in map view. Dashed region (a), (d) outlines higher resolution region of model. NAM – North American plate, PAC – Pacific plate, DF – Denali Fault, PBSZ – Plate Boundary Shear Zone, SMSZ – Southern Model Shear Zone, JdFR – Juan de Fuca Ridge.

sphere, do not include the subducting plate, omit the mantle, or are limited to 2D (Schultz and Aydin, 1990; Lundgren et al., 1995; Bird, 1996; Mazzotti and Hyndman, 2002; Kalbas et al., 2008; Koons et al., 2010; Finzel et al., 2011). The models presented here build on the 3D geodynamic models in Jadamec (2009) and Jadamec and Billen (2010, 2012) by including a Denali fault shear zone in the overriding lithosphere and providing more analysis of how the subducting plate couples into the overriding plate deformation.

2. 3D model design and methods

We construct 3D regional models of the Alaska subduction-transform plate boundary system that include an overriding plate (the North American plate), a subducting plate (the Pacific plate), and the underlying mantle (Fig. 2 and Table 2). The plates are separated by a curvilinear viscous shear zone that follows the shape of the plate interface. The negative thermal buoyancy of the subducting slab drives the flow. No driving velocities are applied to the plates or the slab, rather the models predict the flow velocities for the plates and mantle. These are all instantaneous flow simu-

lations designed to explore the present-day balance of forces, and lithosphere and mantle structure.

2.1. 3D model design using SlabGenerator

The C/C++ code, SlabGenerator (Jadamec, 2009; Jadamec and Billen, 2010, 2012; Jadamec et al., 2012), is used to construct the finite-element mesh, plate boundary interface, and 3D temperature structure used in the geodynamic models of the Alaska subduction-transform system (Sections 2.1.1–2.1.3).

2.1.1. Model domain

The model mesh spans 185° to 240° longitude (from the central Aleutians to eastern British Columbia), 45° to 72° N latitude (from northern Oregon to the Arctic Ocean), and 0 to 1500 km in depth (from the Earth's surface to within the lower mantle) (Figs. 2a, d). The mesh resolution ranges from 0.04° to 0.255°, from 0.0211° to 0.18°, and from 2.35 km to 25 km, respectively, resulting in 960 × 648 × 160 elements (100,413,929 mesh nodes). The finest resolution is centered on south central Alaska (Figs. 2a, d).

Table 2
Summary of model parameters and results.

Model	Rheol.	T _{NAM}	PBSZ (Pa s)	DF (Pa s)	V _{PAC} (°), (cm/yr)	V _{CWB} (°), (cm/yr)	V _{NWB} (°), (cm/yr)	H _{CAKR} (km)	H _{EAKR} (km)
B1n	Newt.	var.	1 × 10 ²⁰	–	332.6, 1.9	306.4, 0.3	270.6, 0.3	-0.3	0.0
B1ndf20	Newt.	var.	1 × 10 ²⁰	1 × 10 ²⁰	332.3, 2.0	309.9, 0.7	277.4, 0.6	0.7	0.3
B1ndf21	Newt.	var.	1 × 10 ²⁰	1 × 10 ²¹	332.3, 2.0	308.7, 0.5	273.7, 0.5	0.8	0.4
B2n	Newt.	var.	1 × 10 ²¹	–	320.4, 0.7	293.4, 0.3	279.7, 0.3	-0.2	0.0
B2ndf20	Newt.	var.	1 × 10 ²¹	1 × 10 ²⁰	320.2, 0.8	298.6, 0.7	281.9, 0.6	1.3	0.4
B2ndf21	Newt.	var.	1 × 10 ²¹	1 × 10 ²¹	320.2, 0.8	298.3, 0.5	279.5, 0.5	1.7	0.5
B6n	Newt.	unif.	1 × 10 ²¹	–	318.5, 0.7	288.6, 0.3	270.5, 0.3	-0.4	0.0
B1c	Comp.	var.	1 × 10 ²⁰	–	339.6, 4.4	306.7, 0.1	281.4, 0.1	0.0	0.1
B1cdf20*	Comp.	var.	1 × 10 ²⁰	1 × 10 ²⁰	339.5, 4.5	311.9, 0.4	301.8, 0.3	0.7	0.5
B1cdf21	Comp.	var.	1 × 10 ²⁰	1 × 10 ²¹	339.4, 4.5	308.3, 0.3	294.8, 0.3	1.0	0.6
B2c	Comp.	var.	1 × 10 ²¹	–	339.5, 2.0	307.6, 0.1	287.8, 0.1	0.0	0.1
B2cdf20*	Comp.	var.	1 × 10 ²¹	1 × 10 ²⁰	339.3, 2.2	312.6, 0.5	306.8, 0.4	0.9	0.5
B2cdf21	Comp.	var.	1 × 10 ²¹	1 × 10 ²¹	339.3, 2.1	309.3, 0.4	302.3, 0.3	1.4	0.8
B6c	Comp.	unif.	1 × 10 ²¹	–	340.4, 2.1	299.9, 0.1	278.0, 0.1	-0.1	0.1

Models vary the viscosity (Newtonian or Composite), the strength of the plate boundary interface (PBSZ), and the strength of the Denali Fault (DF). Models use a maximum yield stress, $\sigma_y(\text{max})$, of 500 MPa and the slab shape, Slab_{E115} from [Jadamec and Billen \(2010, 2012\)](#).

*Indicates preferred models. For reference, a North American thermal structure that is laterally uniform was also run (T_{NAM} uniform versus variable).

V_{PAC} – Pacific plate velocity (at 217.03°, 57.03° N). V_{CWB} – Central Wrangell Block velocity (at 218.03°, 61.78° N).

V_{NWB} – Northern Wrangell Block velocity (at 211.75°, 62.79° N). H_{CAKR} and H_{EAKR} refer to the height of the dynamic topography predicted in the central (208.99°, 63.08° N) and eastern (213.27°, 63.61° N) Alaska Ranges. Only the relative dynamic topography is significant.

2.1.2. Geometry and thermal structure of subducting and overriding plates

The shape and depth extent of the subducting plate is based on Wadati–Benioff zone seismicity, seismic tomography, and seismic reflection data ([Stephens et al., 1984](#); [Page et al., 1989](#); [Boyd and Creager, 1991](#); [Kissling and Lahr, 1991](#); [Moore et al., 1991](#); [Wolf et al., 1991](#); [Zhao et al., 1995](#); [Gudmundsson and Cambridge, 1998](#); [Doser et al., 1999](#); [Ratchkovski and Hansen, 2002](#); [Ferris et al., 2003](#); [Eberhart-Phillips et al., 2006](#); [Qi et al., 2007](#); [Fuis et al., 2008](#)). We use the same slab geometry as Slab_{E115} from [Jadamec and Billen \(2010, 2012\)](#), which contains a two-tiered shape, extending to 325 km beneath the eastern Aleutians and Alaska Peninsula and extending to only 115 km to the east beneath the Wrangell volcanics (Figs. 1 and 2). This slab shape was shown to provide a better fit to the observations of seismic anisotropy in the mantle from [Christensen and Abers \(2010\)](#) ([Jadamec and Billen, 2010](#)).

The temperature of the subducting plate is calculated with a half-space cooling model, in which the thickness of the thermal lithosphere is a function of the plate age ([Parsons and Sclater, 1977](#); [Turcotte and Schubert, 2002](#)). Ages for the unsubducted part of the Pacific plate are from the sea floor age grid of [Müller et al. \(1997\)](#) (Fig. 2a). Ages for the subducted part of the plate are assigned based on the ages of the Pacific plate at the closest point on the trench. A depth-dependent correction factor is applied to the half-space cooling model, based on a length-scale diffusion analysis, to allow the minimum temperature of the slab to increase in the down dip direction, simulating conductive warming of the slab in the mantle ([Jadamec, 2009](#); [Jadamec and Billen, 2010, 2012](#)) (Fig. 2e).

The thermal structure for the overriding North American plate also assumes a half-space cooling model, but uses effective thermal ages as a proxy to capture the variable thickness of the lithosphere ([Jadamec, 2009](#); [Jadamec and Billen, 2010, 2012](#)) (Fig. 2). In this way, the overriding plate is subdivided into four thermal domains: the cordilleran region (effective age of 30 Myr), the magmatic arc (effective age of 10 Myr), the forearc (effective age of 80 Myr), and ancestral North America (effective age of 80 Myr) (Fig. 2). The choice of effective age is based on a synthesis of regional geophysical and geologic observations, including the surface heat flow ([Blackwell and Richards, 2004](#)), location of Neogene volcanism (Alaska Volcano Observatory; [Plafker et al., 1994a](#)), seismic profiles ([Fuis et al., 2008](#)), Moho temperature estimates, major ter-

rane boundaries ([Greninger et al., 1999](#)), and the integrative work characterizing the thermal structure of the lithosphere in western Canada by [Currie and Hyndman \(2006\)](#) and [Lewis et al. \(2003\)](#). To test model sensitivity to the imposed variable thermal structure (and hence laterally variable lithospheric thickness), a second overriding plate thermal structure is constructed using only a single effective age of 30 Myr, comparable to the lithospheric thickness of a warm continental mobile belt ([Blackwell, 1969](#); [Hyndman et al., 2005](#)) (Table 2).

2.1.3. Plate boundary and Denali fault shear zones

The Plate Boundary Shear Zone (PBSZ) is a narrow low viscosity layer that separates the Pacific and North American plates ([Jadamec, 2009](#); [Jadamec and Billen, 2010, 2012](#), [Jadamec et al., 2012](#)) (Fig. 2d and Table 2). The PBSZ is at least 40 km in width and 100 km in depth. The orientation of the PBSZ follows the surface trace of the plate boundaries from [Bird \(2003\)](#) and is spatially variable in depth following the strike and dip of the subducting plate (see Section 2.1.2 for references) and continuous with the vertically-oriented Fairweather–Queen Charlotte transform fault.

We include a Denali fault in a subset of the models (Figs. 2a, d, Fig. 3, and Table 2). The Denali fault is represented by a vertical shear (low viscosity) zone approximately 40 km in width and 70 km in depth. The Denali fault shear zone follows the trace of the Denali fault from [Plafker et al. \(1994a\)](#) giving it an arcuate shape that mimics that of the plate boundary. The westward extent of the Denali fault in the models is approximately 205° longitude, i.e., we do not include the Boss Creek section of the Denali fault, which extends into cover. To the east, the Denali fault shear zone extends to approximately 224° longitude, i.e., it gets cut off just north of Chatham straight where the fault extends into the inlet. In the models, the Denali fault is situated within the imposed cordillera thermal domain, which has a lithospheric thickness of approximately 65 km, making the Denali fault a throughgoing feature in the lithosphere, as in [Freed et al. \(2006\)](#).

2.2. 3D numerical modeling using CitcomCU

The initial 3D plate boundary configuration and thermal structure constructed by SlabGenerator are used as input to CitcomCU, a community viscous flow code developed by [Moresi and Solomatov \(1995\)](#), [Moresi and Gurnis \(1996\)](#), and [Zhong \(2006\)](#).

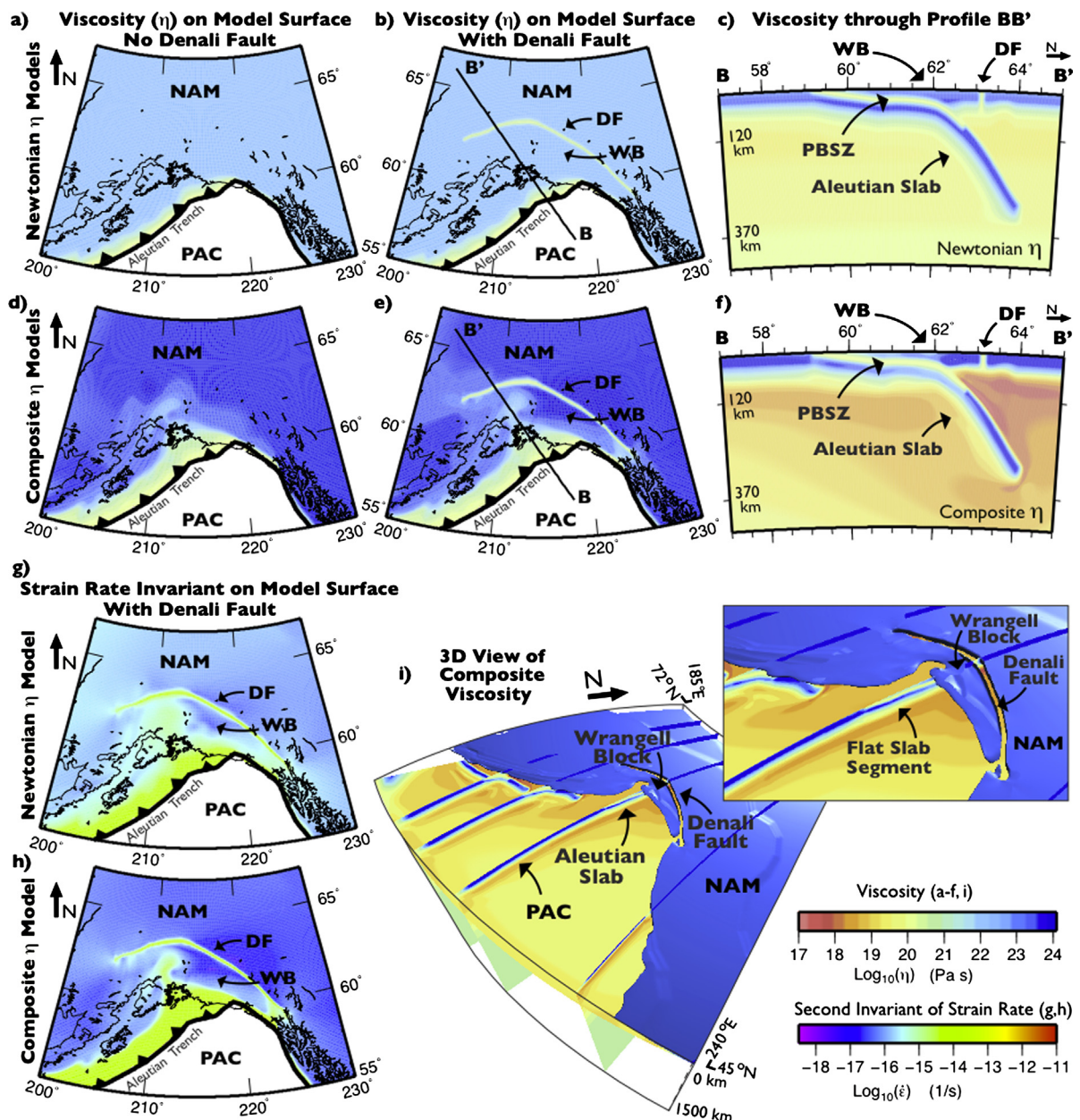


Fig. 3. Viscosity and second invariant of strain rate in model. Viscosity on model surface and in cross section for Newtonian viscosity models (a), (b), (c) and composite viscosity models (d), (e), (f) without and with a Denali fault. Cross sections only shown for models with Denali fault. (g), (h) Second invariant of strain rate on model surface for models in (b), (e) shows lower strain rate in Wrangell block for composite viscosity model. (i) Three-dimensional perspective of viscosity for model in (e), (f) showing formation of Wrangell block located above flat slab and south of Denali fault. PBSZ and DF at 1×10^{20} Pa s, and variable thermal structure for overriding plate. NAM – North American plate, PAC – Pacific plate, DF – Denali Fault, WB – Wrangell Block. Figures shown for subset of model domain, except in (i) which spans entire domain. 2D and 3D-perspective plots in this and other figures made with GMT (Wessel and Smith, 1991) and 3DVisualizer (Kreysel et al., 2006), respectively.

2.2.1. Finite element code, CitcomCU

The 3D models of the Alaska subduction-transform plate boundary system are run using the open source finite element code CitcomCU (Zhong, 2006; Moresi and Solomatov, 1995; Moresi and Gurnis, 1996). CitcomCU solves the conservation of mass and momentum for the velocity and pressure, assuming an incompressible fluid with a high Prandtl number (Moresi and Solomatov, 1995; Zhong, 2006). For the models of the Alaska plate boundary we are interested in the instantaneous force balance, and therefore do not also solve the energy equation. In the viscous flow simulations, reflecting (free-slip) boundary conditions are used on all boundaries. 2D tests were also used to determine the necessary box depth and width in order to minimize boundary condition effects on the flow in the subduction zone.

In post-processing, the height of the dynamic topography, h , is determined assuming $h = \frac{\sigma_{rr}}{\Delta\rho g}$, where $\Delta\rho$ is the difference in mantle and surface density and g is the acceleration due to gravity. σ_{rr} is the vertical stress acting on the underside of model surface calculated by CitcomCU, which includes both the vertical stress due to flow in the mantle transmitted through the lithosphere and the density variations within the lithosphere due to variations in thermal buoyancy, that is, this definition of dynamic topography includes an isostatic component.

2.2.2. Rheological implementation in CitcomCU

We use the composite viscosity, η_{com} , formulation in CitcomCU implemented by Jadamec and Billen (2010, 2012) that assumes the total strain rate is a sum of the contributions from the diffusion

Table 3

Flow law parameters, assuming diffusion and dislocation creep of wet olivine. Values from Hirth and Kohlstedt (2003).

Var.	Description	Creep _{df}	Creep _{ds}
A	Pre-exponential factor	1.0	9×10^{-20}
n	Stress exponent	1	3.5
d	Grain size (μm)	10×10^3	–
p	Grain size exponent	3	–
C_{OH}	OH concentration ($\text{H}/10^6 \text{ Si}$)	1000	1000
r	Exponent for C_{OH} term	1	1.2
E	Activation energy (kJ/mol)	335	480
V	Activation volume (m^3/mol)	4×10^{-6}	11×10^{-6}

and dislocation creep deformation mechanisms which leads to the following form for the composite viscosity (Hall and Parmentier, 2003; Billen and Hirth, 2007)

$$\eta_{\text{com}} = \frac{\eta_{\text{df}}\eta_{\text{ds}}}{\eta_{\text{df}} + \eta_{\text{ds}}}. \quad (1)$$

The viscosity due to diffusion creep, η_{df} , and that due to dislocation creep, η_{ds} , are defined according to the experimentally-derived flow law for olivine aggregates,

$$\eta_{\text{df,ds}} = \left(\frac{dp}{AC_{\text{OH}}^r} \right)^{\frac{1}{n}} \dot{\varepsilon}^{\frac{1-n}{n}} \exp \left[\frac{E + PV}{nR(T + T_{\text{ad}})} \right], \quad (2)$$

where P is the lithostatic pressure, R is the universal gas constant, T is non-adiabatic temperature, T_{ad} is the adiabatic temperature (with an imposed gradient of 0.3 K/km), and A , n , d , p , C_{OH} , r , E , and V are as defined in Table 3, assuming no melt is present and deformation under a fixed stress (Hall and Parmentier, 2003; Hirth and Kohlstedt, 2003). Where strain-rates are high, the dislocation creep deformation mechanism leads to a local reduction in the viscosity. The lower mantle viscosity in the model is Newtonian (diffusion creep only) and uses a larger effective grain size (70 mm) in order to create a viscosity jump by a factor of 30 from the upper to lower mantle (Mitrovica, 1996; Hager, 1984; Billen and Hirth, 2007).

To allow for plastic yielding, where the stress exceeds that predicted by laboratory experiments, a depth-dependent yield stress, σ_y , is used that increases from 0.1 MPa at the surface to a maximum value of 500 MPa (Kohlstedt et al., 1995; Weidner et al., 2001; Hirth, 2002; Billen and Hirth, 2005, 2007; Jadamec and Billen, 2010, 2012). In addition, the two imposed shear zones, the PBSZ and Denali fault shear zone, mapped onto the mesh by Slab-Generator are smoothly blended into the background viscosity in CitcomCU using the modifications to CitcomCU by Jadamec and Billen (2010, 2012) and Jadamec et al. (2012).

3. Results

We now show the effect of varying the viscosity (Newtonian versus composite), the strength of the plate boundary interface (PBSZ), and the presence and strength of the Denali fault on the viscosity structure, strain rate, velocity, and dynamic topography in south-central Alaska (Table 2).

3.1. Viscosity structure and plate mantle coupling

Models that use the Newtonian rheology are characterized by a uniform viscosity on the model surface, with values on the order of 10^{22} Pa s (Figs. 3a–c). High strain rates (10^{-14} s^{-1} to 10^{-15} s^{-1}) occur in south-central Alaska above the flat slab and along the length of the Cook Inlet–Susitna Basin decreasing to background values on the order of 10^{-16} s^{-1} (Fig. 3g). The viscosity in the mantle decreases with depth due to increasing temperature, but is laterally uniform within the mantle with values on the order of 10^{20} to 10^{21} Pa s (Fig. 3c).

Models using the composite viscosity are characterized by a weakening of the plate margin (10^{20} to 10^{21} Pa s) and strengthening of the plate interior (10^{24} Pa s) (Figs. 3d–f), consistent with previous models using a non-linear (stress-dependent) rheology (Zhong et al., 1998). The range in strain rate is also larger in the composite viscosity models, with strain rates in south-central Alaska above the flat slab as high as 10^{-13} s^{-1} that decrease rapidly toward the plate interior to values on the order of 10^{-17} s^{-1} (Fig. 3h). The most prominent regions of low viscosity occur above the flat slab close to the trench and as a diffuse band extending northwest from Prince William Sound to the Denali fault (Figs. 3d, e). These low viscosity regions do not occur in the models using the Newtonian viscosity (Figs. 3a, b).

In models using the composite viscosity, a laterally variable viscosity also develops in the mantle (Fig. 3f). Viscosities in the mantle wedge and beneath the subducting plate are locally reduced by several orders of magnitude (to on the order of 10^{18} Pa s to 10^{17} Pa s) with the lowest values coinciding with the regions of highest strain rate (Jadamec and Billen, 2010, 2012) (Figs. 3f, i). Viscosity reductions on this order (10^{18} Pa s) beneath south-central Alaska are consistent with upper mantle viscosities predicted by post-seismic relaxation models (Freed et al., 2006) of the 2002 Denali fault event and with asthenospheric viscosities from glacial isostatic adjustment models in southeast Alaska (Elliott et al., 2010; Sato et al., 2011). The formation of the laterally variable mantle viscosity in models using the composite viscosity formulation leads to laterally variable coupling of the lithosphere to the upper mantle in the subduction zone (Fig. 3f).

3.2. Formation of Wrangell block in models with a Denali fault

For models that include a Denali fault, a semi-isolated segment within the overriding plate forms that is bounded to the south by the Aleutian trench, underlain by the plate interface (PBSZ), and bounded to the north and east by the Denali fault (Figs. 3b, c, e, f, i). This region correlates to what has been identified in geologic and geodetic studies as the Wrangell block or southern Alaska block, and is conceptually similar to a fore-arc sliver (Lahr and Plafker, 1980; Freymueller et al., 2008; Haussler, 2008; Kalbas et al., 2008; Freymueller and Elliot, 2011) (Fig. 3i). For convenience, will refer to this region hereafter as the Wrangell block (Fig. 3i).

In both the Newtonian and composite viscosity models, the Wrangell block is characterized by a low strain-rate interior (10^{-16} s^{-1} to 10^{-18} s^{-1}) (Figs. 3g, h), with relatively lower strain rates and higher viscosities in the Wrangell block interior for models using the composite viscosity (Figs. 3e, h). The viscosity and strain-rate plots suggest that a western boundary to the Wrangell block forms in models with the composite viscosity. The boundary is defined by the northwest trending diffuse band of high strain rate and low viscosity that correlates with the westward steepening of the flat slab in the subsurface (Figs. 3e, f, h, i). This low viscosity region does not occur in the Newtonian viscosity models (Figs. 3b, c), leaving the western boundary of the Wrangell block poorly defined in the Newtonian viscosity models.

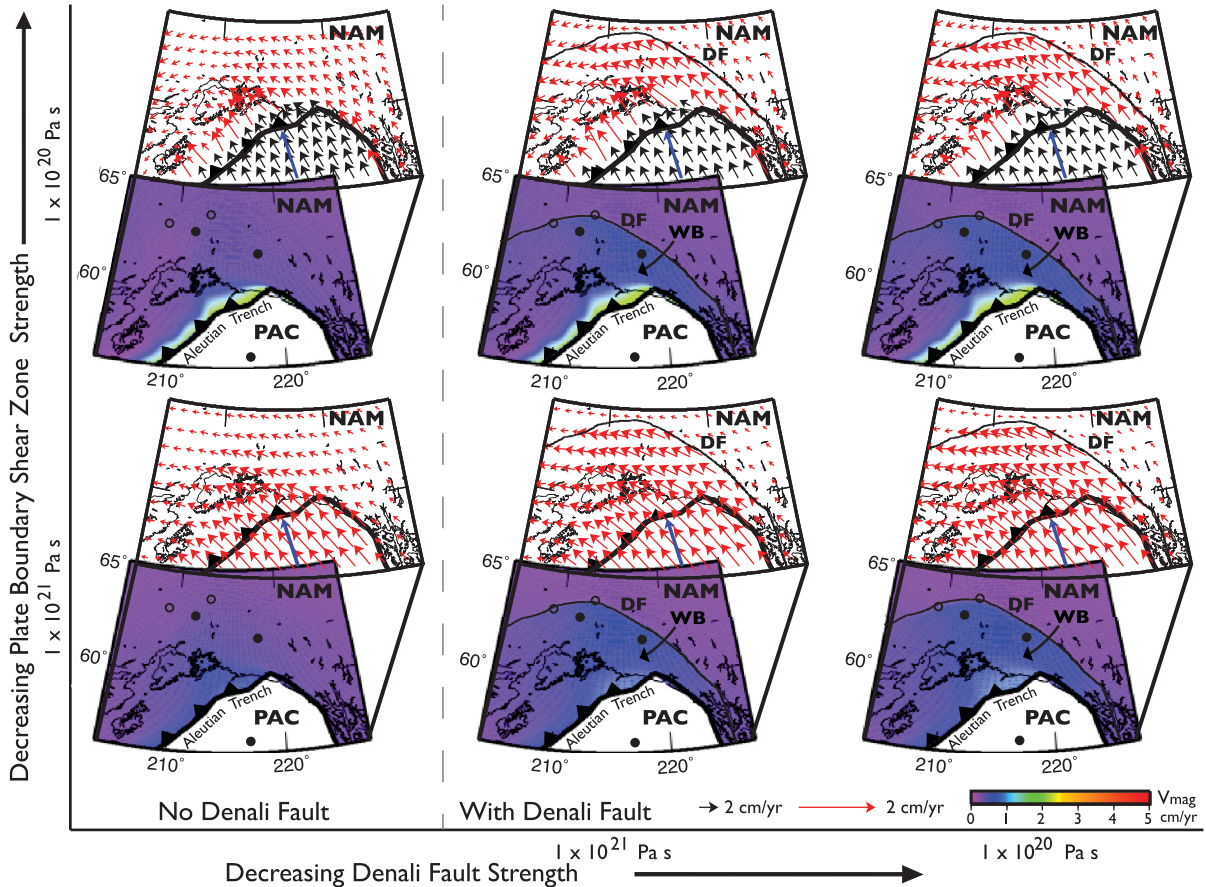


Fig. 4. Predicted velocity vectors and horizontal velocity magnitude (V_{mag}) on model surface for Newtonian viscosity models. Plots shown as a function of decreasing Denali fault strength (horizontal axis) and plate boundary shear zone strength (vertical axis). Models with Denali fault show domain of fast velocities located south of Denali fault, with a counterclockwise sense of rotational motion. Two arrow scales are used to show predicted velocity vectors for subducting Pacific plate (faster) and overriding North American plate (slower) on same plot. Horizontal velocities faster than 1.25 cm/yr shown with black arrow. Observed NUVEL-1A Pacific motion vector assuming North America fixed (DeMets and Dixon, 1999) shown in blue (uses same scale as black arrow). Solid (open) circles denote locations of velocity (dynamic topography) results listed in Table 2. Models use variable thermal structure in overriding plate. NAM – North American plate, PAC – Pacific plate, DF – Denali Fault, WB – Wrangell Block. Figures shown for subset of model domain. (For interpretation of the references to color in this figure legend, the reader is referred to the web version of this article.)

3.3. Predicted Pacific plate motion

In the geodynamic models of the Alaska subduction zone, the negative buoyancy of the slab drives the flow, and therefore the models solve for the velocity of the subducting plate as well as the overriding plate (Table 2). The velocity of the subducting Pacific plate varies as a function of the viscosity structure, either Newtonian (Fig. 4) or composite (Fig. 5), and the coupling along the plate interface (Table 2). Decreasing the plate boundary strength from 10^{21} Pa s to 10^{20} Pa s increases the Pacific plate speed by approximately a factor of 2, for both the Newtonian and composite viscosity models (Figs. 4 and 5 and Table 2). The largest velocities predicted for the Pacific plate occur in the non-Newtonian models with values offshore Alaska of 4.5 cm/yr (Fig. 5), which is comparable to the observed NUVEL-1A Pacific motion vector of 5.2 cm/yr assuming North America fixed (DeMets and Dixon, 1999).

The predicted direction of the Pacific plate varies from west-northwest to north-northwest, with the more northerly directions in models that use the composite viscosity (Figs. 4 and 5 and Table 2). The more northerly Pacific plate motion in models using the composite viscosity is due, in part, to a decreased resistance to slab sinking due to the weakening effects of the strain-rate dependent rheology in the mantle, allowing for the weight of the slab closer to the slab edge to contribute to the slab pull (Jadamec and Billen, 2010, 2012).

3.4. Predicted overriding plate and Wrangell block motion

In models that do not include a Denali fault, the predicted motion of the overriding plate in south-central Alaska is west-northwest for models using the Newtonian viscosity (Fig. 4, left column) and north-northwest for models using the composite viscosity (Fig. 5, left column) (Table 2). The horizontal velocity magnitude in the overriding plate is largest close to the plate boundary. The velocity gradient is sharper for models using the composite viscosity, with values of up to almost 5 cm/yr close decreasing to less than 0.25 cm/yr over less than 150 km (Fig. 5). The faster velocities in the composite viscosity models occur near the plate boundary in the thinnest part of the upper plate where the viscosities are reduced.

The predicted velocity in the overriding plate is markedly different in models that include a Denali fault. For models that include a Denali fault, the Wrangell block moves as a coherent region of relatively high and uniform velocity, semi-independent from that of the rest of the North American plate (Figs. 4 and 5 and Table 2). This effect is observed in both the Newtonian and composite viscosity models, with the overall sense of motion of the Wrangell block tracking the Pacific plate motion and guided by the curvature of the Denali fault.

For models using the Newtonian viscosity (Fig. 4 and Table 2), the Wrangell block is characterized by counterclockwise rotational motion, with the rotational motion following the curvature of the

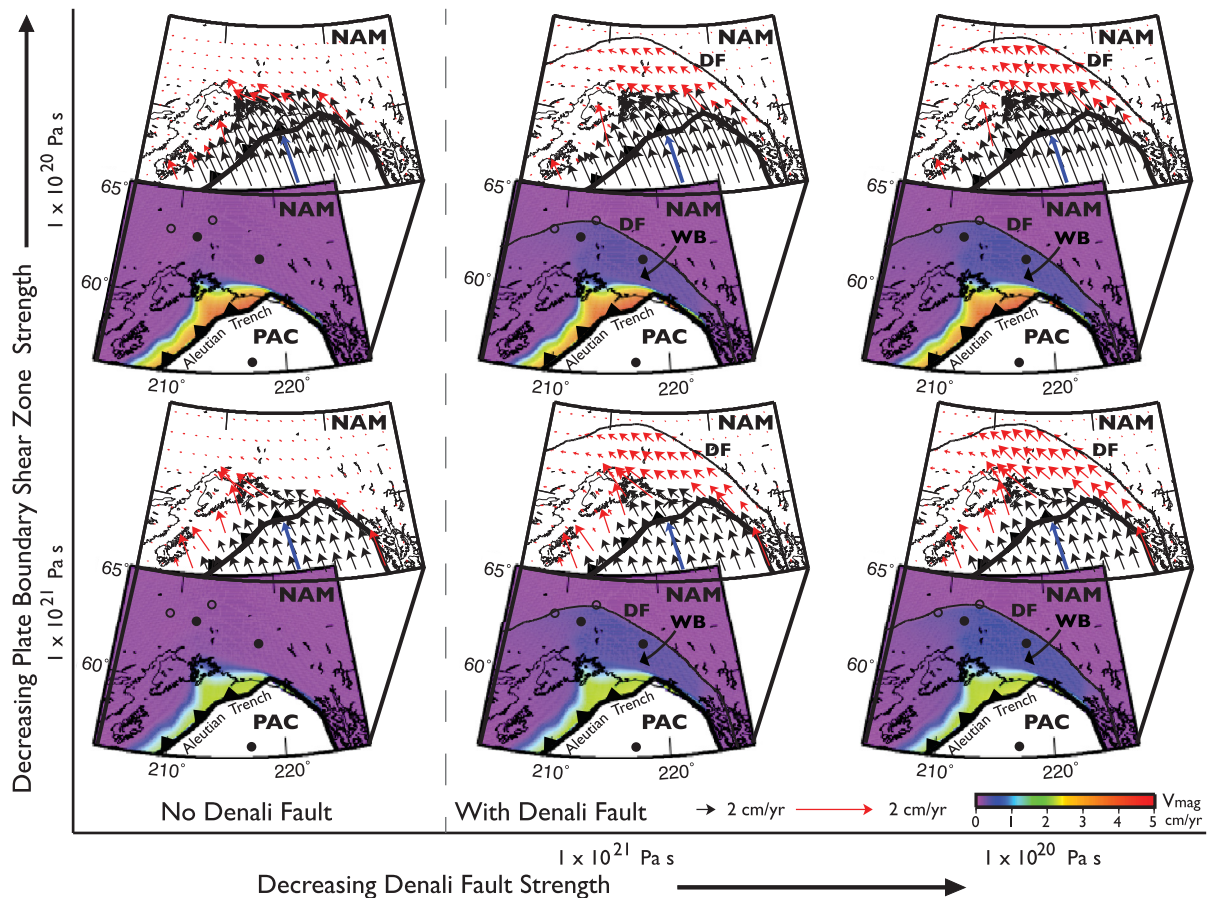


Fig. 5. Predicted velocity vectors and horizontal velocity magnitude (V_{mag}) on model surface for composite viscosity models. Plots shown as a function of decreasing Denali fault strength (horizontal axis) and plate boundary shear zone strength (vertical axis). Models with Denali fault show domain of fast velocities located south of Denali fault, with a northwest sense of translational motion. Two arrow scales are used to show predicted velocity vectors for subducting Pacific plate (faster) and overriding North American plate (slower) on same plot. Horizontal velocities faster than 1.25 cm/yr shown with black arrow. Observed NUVEL-1A Pacific motion vector assuming North America fixed (DeMets and Dixon, 1999) shown in blue (uses same scale as black arrow). Solid (open) circles denote locations of velocity (dynamic topography) results listed in Table 2. Models use variable thermal structure in overriding plate. NAM – North American plate, PAC – Pacific plate, DF – Denali Fault, WB – Wrangell Block. Figures shown for subset of model domain. (For interpretation of the references to color in this figure legend, the reader is referred to the web version of this article.)

Denali fault. In these models, increasing the plate boundary coupling leads to more westward motion of the Pacific plate and hence to more westward (and less rotational) motion of the western part of the Wrangell block. For models using the composite viscosity (Fig. 5 and Table 2), the motion of the Wrangell block is predominantly translational and directed toward the northwest, resulting in oblique motion (including compressional motion) of the Wrangell block with respect to the northern bend in the Denali fault. The predicted translational motion for the Wrangell block is consistent with Quaternary slip rates along the Denali fault (Matmon et al., 2006; Mériaux et al., 2009) and Quaternary fault history of thrust fault development on either side of the Denali fault (Haeussler, 2008; Bemis et al., 2012), but is less consistent with the geodetic data which show fault parallel motion of the Wrangell block along much of the length of the Denali fault (Freymueller et al., 2008). For both the Newtonian and composite viscosity models, decreasing the strength of the Denali fault from 10^{21} Pas to 10^{20} Pas increases the velocity within the Wrangell block, with maximum values on the order of 1.0 cm/yr.

The velocity of the Wrangell block decreases sharply across the Denali fault, with the transition occurring over a distance of less than 40 km and with a larger velocity gradient in models using the composite viscosity (Figs. 4 and 5). In the westward direction, the change in velocity magnitude from the Wrangell block toward the plate interior is more gradual, occurring over several hundred

kilometers, as the Denali fault does not bound the west side of the Wrangell block, but only the east and north sides. The velocity gradient in the westward direction is larger in the composite viscosity models, where the north-south trending band of low viscosity forms a gradational westward edge to the Wrangell block. The decrease in velocity to the west correlates to where the flat slab separates from the overriding plate, indicating the reduction in Wrangell block velocity is due in part to the loss of traction with the subducting plate. The westward decrease in Wrangell block velocity in both the Newtonian and composite viscosity models implies a westward decrease in motion along the northern trace of the Denali fault, which is consistent with the observed decrease in strike-slip motion from the eastern to northern strands of the Denali fault from geologic studies (Matmon et al., 2006; Mériaux et al., 2009).

3.5. Regional dynamic topography in south-central Alaska

There are several features that emerge in the dynamic topography regardless of the rheology used or the inclusion of the Denali fault. The overall pattern is a suite of highs and lows that emerge in south-central Alaska within approximately 600 km of the plate boundary and following the overall curvilinear shape of the subducted Pacific slab (Fig. 6 and Table 2). As these models do not contain an imposed background mantle flow field, the dynamic topography results here are due to the dynamics of the

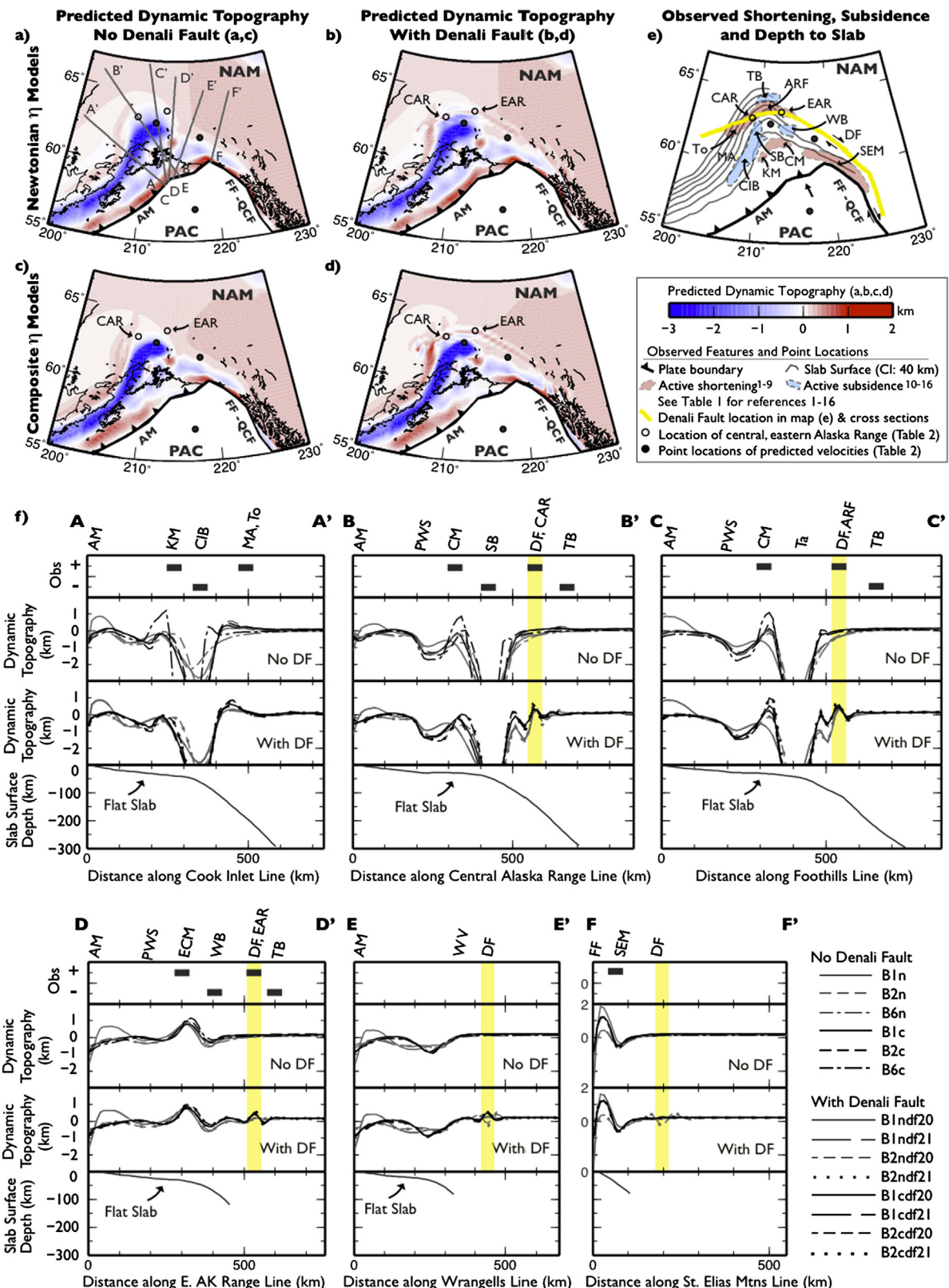


Fig. 6. Predicted dynamic topography, observed shortening and subsidence, and slab geometry. Predicted dynamic topography on model surface for Newtonian viscosity models (a), (b) and composite viscosity models (c), (d) without and with a Denali fault. (a), (b), (c), (d) Plate Boundary Shear Zone and Denali fault shear zone at 1×10^{20} Pa s, and variable thermal structure used in overriding plate. Only relative dynamic topography is significant. Dynamic topography color scale saturates at -3 km. (e) Observed active shortening and subsidence in south-central Alaska from Table 1 superimposed on contours of slab depth. (f) Cross sections of predicted dynamic topography for all models (center graphs), observed shortening (+) and subsidence (-) (upper graphs) from Table 1, and depth to slab surface (lower graphs) from (Jadamec and Billen, 2010, 2012) and references therein. ARF – Alaska Range Foothills, AM – Aleutian Megathrust, CAR – Central Alaska Range, CIB – Cook Inlet Basin, CM – Chugach Mountains, DF – Denali Fault, EAR – Eastern Alaska Range, ECM – Eastern Chugach Mountains, FF – Fairweather Fault, QCF – Queen Charlotte Fault, KM – Kenai Mountains, MA – Magmatic Arc, PWS – Prince William Sound, SEM – St. Elias Mountains, Ta – Talkeetna Mountains, To – Tordrillo Mountains, TB – Tanana Basin, WB – Wrangell Basin, WV – Wrangell Volcanics. Map and cross sections shown for a subset of the model domain.

density driven flow of the slab and overriding plate thermal structure.

The most prominent low occurs as an elongate region following the Cook Inlet Basin and arcing eastward into the Wrangell Basin (Fig. 6). This prominent low predicted by the geodynamic models spatially coincides with the observed young subsidence in the Cook Inlet and Susitna Basins on the west and the Wrangell Basin on the east (Kirschner and Lyon, 1973; Hartman et al., 1974; Dallegge and Layer, 2004; Meyer and Boggess, 2003a, 2003b) (Figs. 6e, f and Table 1). The predicted basin locations occur above the ~60 km slab depth contour, which is approximately equal to the depth of the base of the overriding plate lithosphere for the Cordilleran domain in the models. At this depth, the slab also increases in dip, indicating that the basins correlate to where the slab begins to steepen and separate from the overriding plate (Fig. 6f).

The Talkeetna mountains are located between the Susitna and Wrangell Basins (Fig. 6e, f (cross section CC')), suggesting that the models may over-predict the negative dynamic topography in the central part of this arcuate low dynamic topography feature. However, the low-T thermochronologic data from this region show variable cooling histories and suggest the regional uplift may predate the modern slab configuration (Hoffman and Armstrong, 2006; Hacker et al., 2011). In addition, this region is where seismic data suggest the subducted Yakutat plateau may be located at depth (Ferris et al., 2003; Christeson et al., 2010), which would be expected to reduce negative dynamic topography in the central part of this arcuate feature.

The most prominent regions of positive dynamic topography predicted by the models, regardless of the rheology used or the inclusion of the Denali fault, include an elongate arcuate region adjacent to the Aleutian megathrust and juncture with the northern Fairweather–Queen Charlotte fault, an isolated region in the vicinity of the eastern Chugach Mountains, an elongate region in the western Chugach Mountains and on the east side of the Kenai Peninsula in the Kenai Mountains, and an arcuate region along the modern magmatic arc (Fig. 6).

The predicted high at the juncture of the Aleutian megathrust with the northern Fairweather–Queen Charlotte transform fault coincides with the observed young exhumation in the St. Elias mountains (Enkelmann et al., 2009) and implies that the St. Elias mountains arise in part from the plate boundary geometry in that they are positioned in the apex of the plate boundary corner of a convergent margin (Table 1 and Fig. 6 and cross section FF'). The predicted high in dynamic topography in the eastern Chugach Mountains corresponds to a region of young exhumation (Spotila et al., 2004; Ferguson et al., 2012) suggesting the flat slab plays a role in the uplift in this region (Table 1 and Fig. 6). The elongate region of predicted high dynamic topography in the western Chugach Mountains and in the Kenai Mountains coincides with the dramatic change in relief from the Cook Inlet Basin to the west to the glaciated landscape on the east side of the Kenai Peninsula and indicates that the flat slab subduction provides a mechanism for the young exhumation recently documented in this region by Arkle et al. (2013) (Table 1 and Figs. 1, 6).

In the Alaska Peninsula, the high in the dynamic topography correlates to the observed magmatic arc and results from upwelling along the imposed thinner lithosphere of the magmatic arc thermal domain in the overriding plate (Figs. 1, 6). Note that, models that do not include a Denali fault do not produce localized positive dynamic topography far inboard from the plate boundary in the vicinity of the central Alaska Range, despite the presence of the flat slab, indicating that the flat slab alone is not enough to produce the mountain building in the central Alaska range (Figs. 6a, c, f).

3.6. Dynamic topography along the Denali fault and uplift of the central Alaska Range

The inclusion of a Denali fault has a significant impact on localizing deformation inboard of the plate boundary (Figs. 6b, d, f and Table 2). For models that include a Denali fault, localized positive dynamic topography is predicted along the northwestern arc of the Denali fault, with the highs more pronounced in models using the composite viscosity (Fig. 6b, d and cross sections BB' and CC' and Table 2). Positive dynamic topography is also predicted along the northeastern trace of the Denali fault, with the highs extending along a greater length of the Denali fault in models using the composite viscosity (Figs. 6b, d and cross sections DD' and EE' and Table 2). The predicted localized uplift along the northern arc in the Denali fault corresponds with the locations of active exhumation in the central and eastern Alaska ranges as well as with active shortening in the northern foothills of the central Alaska Range (Fitzgerald et al., 1993, 1995; Bemis and Wallace, 2007; Bemis et al., 2012; Benowitz et al., 2011) (Figs. 6e, f and Table 1).

Thus, these models indicate that both the Denali fault and the flat slab are required to produce the mountain building in the central Alaska Range. It is important to emphasize that for models that do incorporate a Denali fault, positive dynamic topography is not predicted along the entire trace of the imposed fault, but rather is concentrated at its northern bend indicating that imposing a localized lithospheric shear zone alone will not by default produce uplift, but that the forces in the system must also be correct to produce the localized positive topography corresponding to the exhumation in the Alaska Range (Fig. 6).

Models that include a Denali fault also predict greater positive dynamic topography near the intersection of the Denali fault with the northernmost magmatic arc of the Alaska Peninsula (Figs. 6b, d). The positive dynamic topography is more pronounced in models using the composite viscosity. The predicted highs here correlate approximately with the location of observed exhumation in the Tordrillo Mountains (Haeussler, 2008; Benowitz et al., 2012), suggesting a tectonic as well as magmatic origin for uplift along the northernmost magmatic arc in the Alaska Peninsula (Figs. 6e, f (cross section AA')).

4. Discussion

We present 3D numerical models of the Pacific–North American plate in Alaska that include an overriding plate, the underlying mantle, and a slab with an observationally based geometry that is driven by its negative buoyancy rather than by an imposed plate velocity. Thus, these are among the first models to demonstrate the subducting Pacific plate can dynamically drive deformation in south-central Alaska (Fig. 7). This suggests an alternate mechanism for deformation in south-central Alaska to kinematic models (Finzel et al., 2011) that do not test the effect of a slab but instead predict that relative motion of the North American and Bering plates controls the deformation. In particular, the models presented here emphasize the importance of the flat slab, consistent with previous studies that found a correlation of flat slab subduction with increased plate coupling and seismic deformation in the upper plate in South America, Japan, and Alaska (Gutscher et al., 2000; Gutscher and Peacock, 2003). The models further show that a large-scale intra-continental shear zone, such as the Denali fault, can have a significant effect when occurring in a flat slab subduction tectonic environment (Fig. 7).

Numerous hypotheses have been previously put forth to explain the far-field exhumation and mountain building in the Alaska Range (Schultz and Aydin, 1990; Fitzgerald et al., 1993; Plafker et al., 1994a). These geometric and kinematic arguments provide valuable insights based on the geology, but had not previously

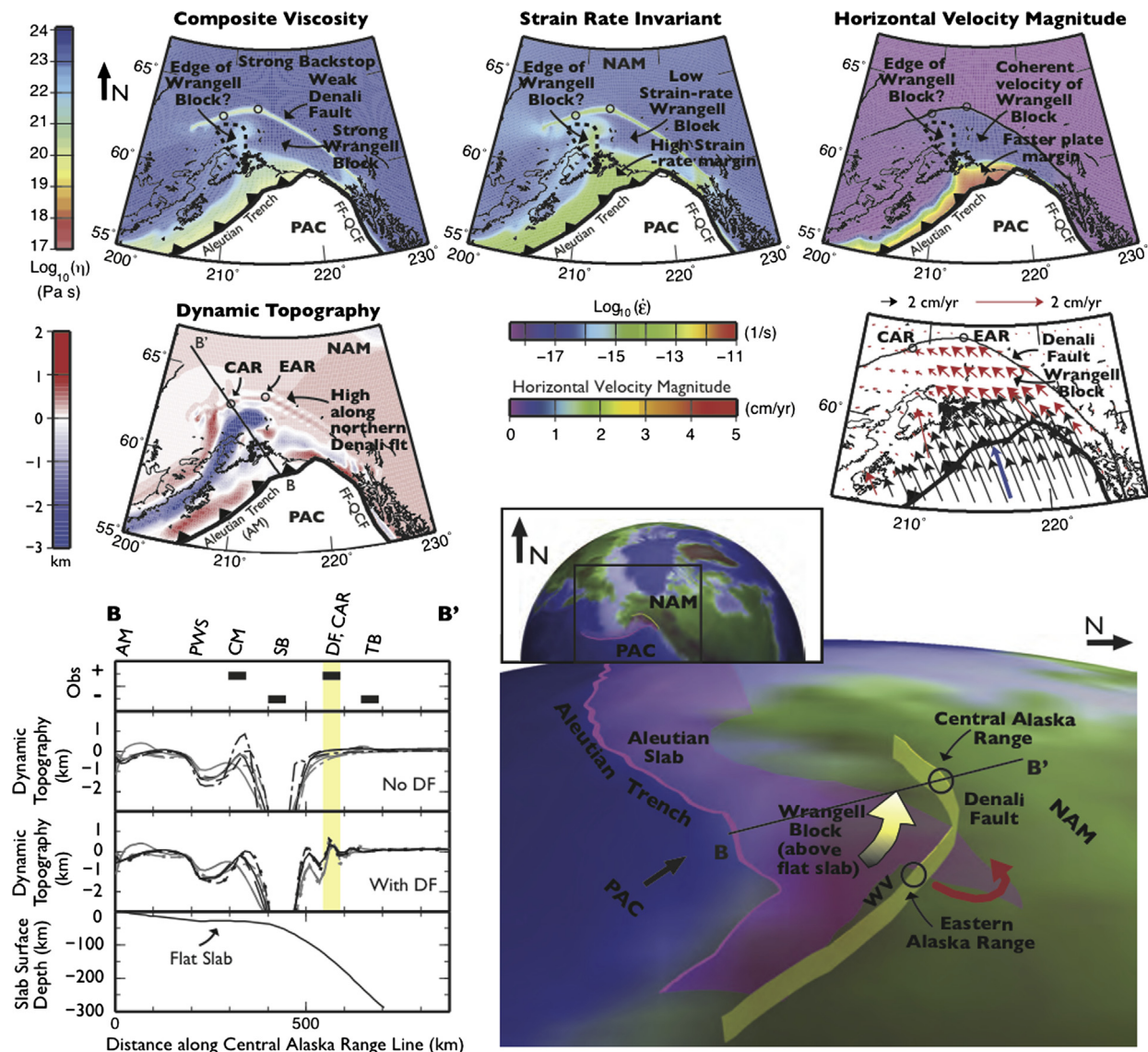


Fig. 7. Results for preferred model (B1cdf20 in Table 2) with cartoon demonstrating how the modern tectonic configuration can generate uplift of the central Alaska Range. Figures show the interrelation between the subducting plate, Denali fault, formation of the Wrangell block, and the lithospheric deformation in south-central Alaska. Open circles show location of central and eastern Alaska Range. Yellow arrow shows schematic motion of Wrangell block from Freymueller et al., 2008, coinciding with where the numerical modeling results indicate the Wrangell block is coupled to the flat surface of the downgoing slab. Red arrow in cartoon shows toroidal mantle flow around slab edge from (Jadamec and Billen, 2010, 2012), indicating partial decoupling of mantle wedge from back-arc. Note, the Wrangell Volcanics (WV) are located above the slab edge return flow suggesting the associated upwelling could contribute to their anomalous (adakitic) geochemistry (Preece and Hart, 2004; Jadamec and Billen, 2012; Durance et al., 2012). Cross section inset shows predicted dynamic topography for all models. Label abbreviations same as in Fig. 6.

been tested with a geodynamic model that includes both a subducting plate and overriding plate to determine if the present balance of forces in the subduction zone can actually produce the localized mountain building inboard of the plate boundary. The models here show the localized intra-continental mountain building in the central Alaska Range, responsible for the tallest mountain in the North American continent, Mt. McKinley, can be produced by the modern flat slab configuration in Alaska combined with a vertical lithosphere scale shear zone and a non-Newtonian rheology (Figs. 1, 6, and 7).

The 3D geodynamic models of the Alaska subduction zone demonstrate that the predicted motion of the overriding plate varies as a function of the predicted subducting plate velocity, indicating the overriding plate in south-central Alaska is tracking the motion of the subducting Pacific plate. Thus, the overall effect of including the Denali fault and using the composite viscosity is to isolate a portion of the overriding plate such that it can now be translated by flat slab subduction into a North American continental

backstop, with the central Alaska Range located at this juncture (Figs. 3 and 7). Moreover, the results provide evidence from a geodynamic model that a change in plate motion to a more northerly plate vector at 5–6 Ma could trigger the onset of rapid exhumation in the central Alaska Range at 5–6 Ma as suggested by Fitzgerald et al. (1993, 1995), with the more northerly Pacific motion (Cox and Engebretson, 1985) being translated to the upper plate via coupling between the flat slab and fore-arc sliver.

Thus, these models illustrate how lateral variations in coupling in a subduction zone can affect upper plate deformation, with coupling of the base of the overriding plate to the surface of the subducting plate transitioning to partial de-coupling of the overriding plate to the low viscosity mantle wedge in the back arc (Figs. 3 and 7). This variable coupling provides a mechanism for the semi-independent motion of fore-arc slivers (Fitch, 1972) and the lateral translation of continental fragments suggested by models of escape tectonics (England and Molnar, 1990; Avouac and Tapponnier, 1993; Yin et al., 2002; Redfield et al.,

2007; Thatcher, 2009). In the Alaska case, the Wrangell block is the fore-arc sliver and is driven by the underlying flat slab, with the models here predicting transpressional motion, as in Dewey et al. (1998), rather than full partitioning of the oblique convergence vector suggested by Fitch (1972).

In Alaska, it has been a question whether and, if so, where there is a western boundary to the Wrangell block. A western boundary to the Wrangell block emerges in the models that use a composite viscosity (Figs. 3 and 7) and correlates with an observed north-south trending band of seismicity located approximately along the Cook Inlet–Susitna Basins (Page et al., 1991). Thus, the modeling results imply the western edge of the Wrangell block and associated band of seismicity are due in part to weakening and deformation in the overriding plate as it accommodates the decoupling between the subducting and overriding plates where the slab steepens to the west. This decoupling zone could reconcile the northwest directed Wrangell block motion predicted by the composite viscosity models with the south directed Bering block motion in western Alaska indicated by the GPS (Cross and Freymueller, 2008; Freymueller et al., 2008) and expected because the central Aleutian trench is rolling back (Schellart et al., 2008).

In terms of the eastern boundary of the Wrangell block, it is interesting to note that although the predicted velocities are sub-parallel to the eastern Denali fault, the models show a change in the form of the predicted dynamic topography along the length of the Denali fault approximately where the Totschunda fault intersects with the Denali fault (Figs. 1, 6, and 7). In particular, the models do not predict the localized high dynamic topography along the Denali fault south of the Totschunda fault – Denali fault interaction, even though a low viscosity shear zone is imposed along the Denali fault in this region of the model (Figs. 1, 6, and 7). This suggests a change in stress in this region of the Totschunda fault and may have implications for an incipient boundary connecting the Totschunda fault to the Fairweather–Queen Charlotte transform fault (Lahr and Plafker, 1980; Kalbas et al., 2008).

The 3D numerical modeling of the Pacific–North American plate boundary in Alaska show that models with the composite viscosity structure provide a better fit to Pacific plate motions and predict both northwest convergence across the northern bend in the Denali fault and more pronounced positive dynamic topography along the Denali fault, indicating this is the preferred viscosity structure (Figs. 3 and 7). It is pertinent to consider, however, that the models do not contain elasticity nor do they include compositional buoyancy to allow for crustal variations or include feedback with erosion, which can be important (Savage, 1983; Avouac and Burov, 1996; Jadamec et al., 2007). Erosion would be expected to play an important feedback role close to the plate boundary in the Chugach–St. Elias Mountains, although the models indicate the initial uplift would be consistent with a tectonic forcing mechanism.

Elasticity and crustal buoyancy would be expected to broaden the predicted regions of uplift and subsidence. The elastic strength would also permit a greater fraction of the plate boundary forces that are absorbed by the low viscosity plate margin to be translated inboard, possibly resulting in greater convergence across the Denali fault. It is interesting to observe, however, that the broad regions of high strain rate in the overriding plate predicted by models with the composite viscosity are consistent with the patterns observed in the global strain rate map (Kreemer et al., 2003). In addition, the formation of a low viscosity upper plate close to the plate margin, associated with the high strain rates, is consistent with the imposed gradients in plate margin viscosity required to fit global models of plate deformation (Ghosh and Holt, 2012). In Alaska, this region of low viscosity generated in the overriding plate allows for faster velocities near the plate margin, consistent with the observed GPS and which occur over a wavelength

too short to be explained by purely elastic models (Ali and Freed, 2010). This suggests a low viscosity upper plate close to the plate margin that is prone to failure, could be a common feature in subduction zones, due in part to the presence of thin lithosphere above the shallow parts of the subduction zone.

5. Conclusions

We investigate the relative roles of the slab geometry, continental scale faulting, and a non-linear rheology on deformation in the overriding plate using 3D numerical models of the Pacific–North American plate system in Alaska. The results show that large-scale intra-continental faulting combined with flat slab subduction together can drive the first order deformation observed in south-central Alaska. These models address, in terms of global tectonic processes: the formation of semi-independent continental masses or fore-arc slivers, a mechanism for uplift of intra-continental mountain belts, the driving forces that generate major fore-arc basins, and a mechanism for producing adakitic volcanics above a slab edge. In Alaska, these features correlate to the Wrangell or Southern Alaska block, the central and eastern Alaska range, the Cook Inlet–Susitna Basin, and the Wrangell volcanics, respectively. No previous model has simultaneously produced these four tectonic features in Alaska.

Acknowledgements

We thank Donald Turcotte, Louise Kellogg, Donna Eberhart-Phillips, John Dewey, Tatia Taylor, Natasha Ruppert, Jeff Benowitz, Andy Freed, and Wes Wallace for discussions. We thank Jeff Freymueller, Grace Shephard, and an anonymous reviewer for thoughtful reviews of the manuscript. We thank the Computational Infrastructure for Geodynamics for the CitcomCU source code, and Oliver Kreylos and the UC Davis KeckCAVES for the 3D visualization infrastructure and software. The work was supported by a National Science Foundation Postdoctoral Fellowship EAR-1049545 awarded to M. Jadamec and National Science Foundation grant EAR-0537995 awarded to M. Billen and S. Roeske. Roeske also received partial support for this work through NSF EAR 0952834. High resolution models were run on Lonestar, at the Texas Advanced Computing Center through TG-EAR120010 and TG-EAR080015N.

References

- Ali, S.T., Freed, A.M., 2010. Contemporary deformation and stressing rates in southern Alaska. *Geophys. J. Int.* 183 (2), 557–571.
- Arkle, J.C., Armstrong, P.A., Haeussler, P.J., Prior, M.G., Hartman, S., Sendziak, K.L., Brush, J.A., 2013. Focused exhumation in the syntaxis of the western Chugach Mountains and Prince William Sound, Alaska. *Geol. Soc. Am. Bull.* 125 (5–6), 776–793.
- Avouac, J.P., Burov, E.B., 1996. Erosion as a driving mechanism of intracontinental mountain growth. *J. Geophys. Res.* 101 (B8), 17,747–17,769.
- Avouac, J.-P., Tapponnier, P., 1993. Kinematic model of active deformation in central Asia. *Geophys. Res. Lett.* 20 (10), 895–898.
- Bemis, S., Carver, G., Koehler, R., 2012. The Quaternary thrust system of the northern Alaska Range. *Geosphere* 8 (1), 196–205.
- Bemis, S., Wallace, W., 2007. Neotectonic framework of the north-central Alaska Range foothills. *Spec. Pap., Geol. Soc. Am.* 431, 549–572.
- Benowitz, J., Haeussler, P., Layer, P., O’Sullivan, P., Wallace, W., Gillis, R., 2012. Cenozoic tectono-thermal history of the Tordrillo Mountains, Alaska: Paleocene–Eocene ridge subduction, decreasing relief, and late Neogene faulting. *Geochem. Geophys. Geosyst.* 13, Q04009.
- Benowitz, J., Layer, P., Armstrong, P., Perry, S., Haeussler, P., Fitzgerald, P., VanLaningham, S., 2011. Spatial variations in focused exhumation along a continental-scale strike-slip fault: The Denali fault of the eastern Alaska Range. *Geosphere* 7 (2), 455–467.
- Billen, M.I., Hirth, G., 2005. Newtonian versus non-Newtonian upper mantle viscosity: Implications for subduction initiation. *Geophys. Res. Lett.* 32, L19304.
- Billen, M.I., Hirth, G., 2007. Rheological controls on slab dynamics. *Geochem. Geophys. Geosyst.* 8, Q08012.
- Bird, P., 1996. Computer simulations of Alaskan tectonics. *Tectonics* 15 (2), 225–236.

- Bird, P., 2003. An updated digital model of plate boundaries. *Geochem. Geophys. Geosyst.* 4 (3), 1027.
- Blackwell, D.D., 1969. Heat flow in the northwestern United States. *J. Geophys. Res.* 74, 992–1077.
- Blackwell, D.D., Richards, M., 2004. Geothermal map of North America. Scale 1:6,500,000. American Association of Petroleum Geologists.
- Boyd, T., Creager, K., 1991. The geometry of Aleutian subduction: Three dimensional seismic imaging. *J. Geophys. Res.* 96 (B2), 2267–2291.
- Brocher, T.M., Fuis, G.S., Fisher, M.A., Plafker, G., Taber, J.J., Christensen, N.I., 1994. Mapping the megathrust beneath the northern Gulf of Alaska using wide-angle seismic data. *J. Geophys. Res.* 99 (B6), 11663–11685.
- Bruhn, R.L., Pavlis, T.L., Plafker, G., Serpa, L., 2004. Deformation during terrane accretion in the Saint Elias orogen, Alaska. *Geol. Soc. Am. Bull.* 116 (7/8), 771–787.
- Christensen, D.H., Abers, G.A., 2010. Seismic anisotropy under central Alaska from SKS splitting observations. *J. Geophys. Res.* 115, B04315.
- Christeson, G., Gulick, S., van Avendonk, H., Worthington, L., Reece, R., Pavlis, T., 2010. The Yakutat terrane: Dramatic change in crustal thickness across the Transition fault, Alaska. *Geology* 38 (10), 895–898.
- Coleman, M., Hodges, K., 1995. Evidence for Tibetan plateau uplift before 14 Myr ago from a new minimum age for east–west extension. *Nature* 374 (6517), 49–52.
- Cook, K.L., Royden, L.H., 2008. The role of crustal strength variations in shaping orogenic plateaus, with application to Tibet. *J. Geophys. Res.* 113, B08407.
- Cox, A., Engelbreton, D., 1985. Change in motion of the Pacific plate at 5 Myr BP. *Nature* 313, 472–474.
- Cross, R.S., Freymueller, J.T., 2008. Evidence for and implications of a Bering plate based on geodetic measurements from the Aleutians and western Alaska. *J. Geophys. Res.* 113, B07405.
- Currie, C.A., Hyndman, R.D., 2006. The thermal structure of subduction zone back arcs. *J. Geophys. Res.* 111, B08404.
- Dallegge, T., Layer, P., 2004. Revised chronostratigraphy of the Kenai Group from 40Ar/39Ar dating of low-potassium bearing minerals, Cook Inlet Basin, Alaska. *Can. J. Earth Sci.* 41 (10), 1159–1179.
- DeMets, C., Dixon, T.H., 1999. New kinematic models for Pacific–North American motion from 3 Ma to present: Evidence for steady state motion and biases in the NUVEL-1A model. *Geophys. Res. Lett.* 26, 1921–1924.
- Dewey, J., Holdsworth, R., Strachan, R., 1998. Transpression and transtension zones. *Geol. Soc. London Spec. Publ.* 135 (1), 1–14.
- Doser, D.I., Veilleux, A.M., Velasquez, M., 1999. Seismicity of the Prince William Sound region for over thirty years following the 1964 great Alaskan earthquake. *Pure Appl. Geophys.* 154, 593–632.
- Durance, P.M.J., Jadamec, M.A., Falloon, T.J., Nicholls, I.A., 2012. Magmagenesis within the Hunter Ridge Rift zone resolved from olivine-hosted melt inclusions and geochemical modelling, with insights from geodynamic models. *Aust. J. Earth Sci.* 59 (6).
- Eberhart-Phillips, D., Christensen, D.H., Brocher, T.M., Hansen, R., Ruppert, N.A., Haeussler, P.J., Abers, G.A., 2006. Imaging the transition from Aleutian subduction to Yakutat collision in central Alaska, with local earthquakes and active source data. *J. Geophys. Res.* 111, B11303.
- Eberhart-Phillips, D., Haeussler, P.J., Freymueller, J.T., Frankel, A.D., Rubin, C.M., Crawford, P., Ratchkovski, N.A., Anderson, G., Carver, G.A., Crone, A.J., Dawson, T.E., Fletcher, H., Hansen, R., Harp, E.L., Harris, R.A., Hill, D.P., Hreinsdóttir, S., Gibson, R.W., Jones, L.M., Kayen, R., Keefer, D.K., Larsen, C.F., Moran, S.C., Personius, S.F., Plafker, G., Sherrod, B., Sieh, K., Sitar, N., Wallace, W.K., 2003. The 2002 Denali Fault Earthquake: A large magnitude, slip-partitioned event. *Science* 300, 1112–1118.
- Elliott, J.L., Larsen, C.F., Freymueller, J.T., Motyka, R.J., 2010. Tectonic block motion and glacial isostatic adjustment in southeast Alaska and adjacent Canada constrained by GPS measurements. *J. Geophys. Res.* 115, B09407.
- England, P., Houseman, G., 1985. Role of lithospheric strength heterogeneities in the tectonics of Tibet and neighbouring regions. *Nature* 315, 297–301.
- England, P., Molnar, P., 1990. Right-lateral shear and rotation as the explanation for strike-slip faulting in eastern Tibet. *Nature* 344 (6262), 140–142.
- England, P., Houseman, G., Sonder, L., 1985. Length scales for continental deformation in convergent, divergent, and strike-slip environments: Analytical and approximate solutions for a thin viscous sheet model. *J. Geophys. Res.* 90, 3551–3557.
- Enkelmann, E., Zeitler, P., Pavlis, T., Garver, J., Ridgway, K., 2009. Intense localized rock uplift and erosion in the St. Elias orogen of Alaska. *Nat. Geosci.* 2 (5), 360–363.
- Ferguson, K., Armstrong, P.A., Haeussler, P.J., Arkle, J.C., 2012. Thermochronologic constraints on megathrust splay faulting in the transition from strike-slip to convergence in southern Prince William Sound, Alaska. In: Geological Society of America Annual Meeting. In: Geological Society America Abstracts with Programs, vol. 272–10.
- Ferris, A., Abers, G.A., Christensen, D.H., Veenstra, E., 2003. High resolution image of the subducted Pacific (?) plate beneath central Alaska, 50–150 km depth. *Earth Planet. Sci. Lett.* 214, 575–588.
- Finzel, E., Flesch, L., Ridgway, K., 2011. Kinematics of a diffuse North America-Pacific–Bering plate boundary in Alaska and western Canada. *Geology* 39 (9), 835.
- Fitch, T.J., 1972. Plate convergence, transcurrent faults and internal deformation adjacent to southeast Asia and the western Pacific. *J. Geophys. Res.* 77 (23), 4432–4460.
- Fitzgerald, P.G., Sorkhabi, R.B., Redfield, T.F., Stump, E., 1995. Uplift and denudation of the central Alaska Range: A case study in the use of apatite fission track thermochronology to determine absolute uplift parameters. *J. Geophys. Res.* 100 (B10), 20175–20191.
- Fitzgerald, P.G., Stump, E., Redfield, T.F., 1993. Late Cenozoic uplift and Denali and its relation to relative plate motion and fault morphology. *Science* 259, 497–499.
- Forsyth, D., Uyeda, S., 1975. On the relative importance of the driving forces of plate motion. *Geophys. J. R. Astron. Soc.* 43, 163–200.
- Freed, A., Burgmann, R., Calais, E., Freymueller, J., Hreinsdóttir, S., 2006. Implications of deformation following the 2002 Denali, Alaska, earthquake for postseismic relaxation processes and lithospheric rheology. *J. Geophys. Res.* 111, B01401. <http://dx.doi.org/10.1029/2005JB003894>.
- Freymueller, J., Elliott, J., 2011. An improved model for tectonic deformation in Alaska. In: XXV International Union of Geodesy and Geophysics General Assembly, Program Abstracts.
- Freymueller, J.T., Woodard, H., Cohen, S.C., Cross, R., Elliott, J., Larsen, C.F., Hreinsdóttir, S., Zweck, C., 2008. Active deformation processes in Alaska, based on 15 years of GPS measurements. In: Active Tectonics and Seismic Potential of Alaska. In: *Geophys. Monogr.*, vol. 179. American Geophysical Union, pp. 1–42.
- Fuis, G.S., Moore, T.E., Plafker, G., Brocher, T.M., Fisher, M.A., Mooney, W.D., Nokleberg, W.J., Page, R.A., Beaudoin, B.C., Christensen, N.I., Levander, A.R., Lutter, W.J., Saltus, R.W., Ruppert, N.A., 2008. Trans-Alaska crustal transect and continental evolution involving subduction underplating and synchronous foreland thrusting. *Geology* 36, 267–270.
- Ghosh, A., Holt, W., 2012. Plate motions and stresses from global dynamic models. *Science* 335 (6070), 838–843.
- Greninger, M.L., Klemperer, S.L., Nokleberg, W.J., 1999. Geographic Information Systems (GIS) compilation of geophysical, geologic, and tectonic data for the circum-North Pacific. Open-File Report 99-422. United States Geological Survey.
- Gudmundsson, O., Cambridge, M., 1998. A regionalized upper mantle (RUM) seismic model. *J. Geophys. Res.* 103 (B4), 7121–7136.
- Gutscher, M.A., Peacock, S.M., 2003. Thermal models of flat subduction and the rupture zone of great subduction earthquakes. *J. Geophys. Res.* 108 (B1).
- Gutscher, M.A., Spakman, W., Bijwaard, H., Engdahl, E.R., 2000. Geodynamics of flat subduction: Seismicity and tomographic constraints from the Andean margin. *Tectonics* 19 (5), 814–833.
- Hacker, B., Kelemen, P.B., Rioux, M., McWilliams, M.O., Gans, P.B., Reiners, P.W., Layer, P.W., Söderlund, U., Vervoort, J.D., 2011. Thermochronology of the Talkeetna intraoceanic arc of Alaska: Ar/Ar, U–Th/He, Sm–Nd, and Lu–Hf dating. *Tectonics* 30 (1), TC1011.
- Haeussler, P., 2008. An overview of the neotectonics of interior Alaska: Far-field deformation from the Yakutat Microplate collision. In: Active Tectonics and Seismic Potential of Alaska. In: *Geophys. Monogr.*, vol. 179. American Geophysical Union, pp. 83–108.
- Hager, B.H., 1984. Subducted slabs and the geoid: Constraints on mantle rheology and flow. *J. Geophys. Res.* 89 (B7), 6003–6015.
- Hall, C.E., Parmentier, E.M., 2003. Influence of grain size evolution on convective instability. *Geochem. Geophys. Geosyst.* 4 (3).
- Hartman, D.C., Pessel, G.H., McGee, D.L., 1974. Stratigraphy of the Kenai Group, Cook Inlet. Alaska Open File Report, vol. 49. Alaska Division of Geological and Geophysical Surveys.
- Hirth, G., 2002. Laboratory constraints on the rheology of the upper mantle. In: Karato, S., Wenk, H.R. (Eds.), *Plastic Deformation of Minerals and Rocks*. In: *Rev. Mineral. Geochem.*, vol. 51. Mineralogical Society of America, pp. 97–120.
- Hirth, G., Kohlstedt, D., 2003. Rheology of the upper mantle and the mantle wedge: A view from the experimentalists. In: Eiler, J. (Ed.), *Inside the Subduction Factory*. In: *Geophys. Monogr.*, vol. 138. American Geophysical Union, Washington, DC, pp. 83–105.
- Hoffman, M.D., Armstrong, P.A., 2006. Miocene exhumation of the southern Talkeetna Mountains, south central Alaska, based on apatite (U–Th)/He thermochronology. In: 102nd Annual Meeting of the Cordilleran Section, GSA, 81st Annual Meeting of the Pacific Section, AAPG, and the Western Regional Meeting of the Alaska Section, SPE.
- Hyndman, R.D., Currie, C.A., Mazzotti, S.P., 2005. Subduction zone backarcs, mobile belts, and orogenic heat. *GSAToday* 15 (2).
- Jadamec, M.A., 2009. Three-dimensional lithosphere and mantle dynamics: Models of the subduction-transform plate boundary system in southern Alaska. PhD thesis. University of California, Davis.
- Jadamec, M.A., Billen, M.I., 2010. Reconciling surface plate motions and rapid three-dimensional flow around a slab edge. *Nature* 465, 338–342.
- Jadamec, M.A., Billen, M.I., 2012. The role of rheology and slab shape on rapid mantle flow: Three-dimensional numerical models of the Alaska slab edge. *J. Geophys. Res.* 117, B02304.
- Jadamec, M.A., Billen, M.I., Kreylos, O., 2012. Three-dimensional simulations of geometrically complex subduction with large viscosity variations. In: Proceedings of the 2012 Conference on eXtreme Science and Engineering Discovery Environment. Association for Computing Machinery, pp. 1–8.

- Jadamec, M.A., Turcotte, D.L., Howell, P., 2007. Analytic models for orogenic collapse. *Tectonophysics* 435, 1–12.
- Kalbas, J.L., Freed, A.M., Ridgway, K.D., 2008. Contemporary fault mechanics in southern Alaska. *Geophys. Monogr.* 179, 321–336.
- Kirschner, C.E., Lyon, C.E., 1973. Stratigraphic and tectonic development of Cook Inlet Petroleum Province. In: Pitcher, M.G. (Ed.), Arctic Geology. In: AAPG Mem., vol. 19, pp. 396–407.
- Kissling, E., Lahr, J.C., 1991. Tomographic image of the Pacific slab under southern Alaska. *Ectogae Geol. Helv.* 84, 297–315.
- Kohlstedt, D.L., Evans, B., Mackwell, S.J., 1995. Strength of the lithosphere: Constraints imposed from laboratory experiments. *J. Geophys. Res.* 100 (9), 17587–17602.
- Koons, P., Hooks, B., Pavlis, T., Upton, P., Barker, A., 2010. Three-dimensional mechanics of Yakutat convergence in the southern Alaskan plate corner. *Tectonics* 29.
- Kreemer, C., Holt, W., Haines, A., 2003. An integrated global model of present-day plate motions and plate boundary deformation. *Geophys. J. Int.* 154 (1), 8–34.
- Kreylos, O., Bawden, G.W., Bernardin, T., Billen, M.I., Cowgill, E.S., Gold, R.D., Hamann, B., Jadamec, M., Kellogg, L.H., Staadt, O.G., Sumner, D.Y., 2006. Enabling scientific workflows in virtual reality. In: Wong, K.H., Baciu, G., Bao, H. (Eds.), Proceedings of ACM SIGGRAPH International Conference on Virtual Reality Continuum and Its Applications. VRCIA 2006. ACM Press, New York, pp. 155–162.
- Lahr, J.C., Plafker, G., 1980. Holocene Pacific–North American plate interaction in southern Alaska: Implications for the Yakutatka seismic gap. *Geology* 8, 483–486.
- Lallemand, S., Heuret, A., Boutelier, D., 2005. On the relationships between slab dip, back-arc stress, upper plate absolute motion, and crustal nature in subduction zones. *Geochem. Geophys. Geosyst.* 6 (9), Q09006.
- Lewis, T.J., Hyndman, R.D., Fluck, P., 2003. Heat flow, heat generation, and crustal temperatures in the northern Canadian Cordillera: Thermal controls of tectonics. *J. Geophys. Res.* 108 (B6), 2316.
- Lundgren, P., Saucier, F., Palmer, R., Langon, M., 1995. Alaska crustal deformation: Finite element modeling constrained by geologic and very long baseline interferometry data. *J. Geophys. Res.* 100 (B11), 22033–22045.
- Martinod, J., Funicello, F., Faccenna, C., Labanieh, S., Regard, V., 2005. Dynamical effects of subducting ridges: Insights from 3D laboratory models. *Geophys. J. Int.* 163, 1137–1150.
- Matmon, A., Schwartz, D., Haeussler, P., Finkel, R., Lienkaemper, J., Stenner, H., Dawson, T., 2006. Denali fault slip rates and Holocene–late Pleistocene kinematics of central Alaska. *Geology* 34 (8), 645–648.
- Mazzotti, S., Hyndman, R.D., 2002. Yakutat collision and strain transfer across the northern Cordillera. *Geology* 30 (6), 495–498.
- Mériaux, A., Sieh, K., Finkel, R., Rubin, C., Taylor, M., Meltzner, A., Ryerson, F., 2009. Kinematic behavior of southern Alaska constrained by westward decreasing postglacial slip rates on the Denali Fault, Alaska. *J. Geophys. Res.* 114 (B3), B03404.
- Meyer, J., Boggess, P., 2003a. Principal facts for gravity data collected in the Susitna Basin area, southcentral Alaska. Alaska Division of Geological & Geophysical Surveys: Preliminary Investigative Report, vol. 3. 13 pp.
- Meyer, J., Boggess, P., 2003b. Principle facts for gravity data collected in the Copper River basin area, south central Alaska. Alaska Division of Geological & Geophysical Surveys: Preliminary Investigative Report, vol. 2. 12 pp.
- Mitrovica, J.X., 1996. Haskell [1935] revisited. *J. Geophys. Res.* 101 (B1), 555–569.
- Molnar, P., 1988. Continental tectonics in the aftermath of plate tectonics. *Nature* 335 (6186), 131–137.
- Moore, J.C., Diebold, J., Fisher, M.A., Sample, J., Brocher, T., Talwani, M., Ewing, J., von Huene, R., Rowe, C., Stone, D., Stevens, C., Sawyer, D., 1991. EDGE deep seismic reflection transect of the eastern Aleutian arc-trench layered lower crust reveals underplating and continental growth. *Geology* 19, 420–424.
- Moresi, L., Gurnis, M., 1996. Constraints on the lateral strength of slabs from three-dimensional dynamic flow models. *Earth Planet. Sci. Lett.* 138, 15–28.
- Moresi, L.N., Solomatov, V.S., 1995. Numerical investigation of 2D convection with extremely large viscosity variations. *Phys. Fluids* 7 (9), 2154–2162.
- Morra, G., Regenauer-Lieb, K., Giardini, D., 2006. Curvature of oceanic arcs. *Geology* 34 (10), 877–880.
- Müller, R.D., Roest, W.R., Royer, J.Y., Gahagan, L.M., Slater, J.G., 1997. Digital isochrons of the world's ocean floor. *J. Geophys. Res.* 102, 3211–3214.
- Müller, R.D., Sdrolias, M., Gaina, C., Roest, W.R., 2008. Age, spreading rates, and spreading asymmetry of the world's ocean crust. *Geochem. Geophys. Geosyst.* 9 (4).
- Nokleberg, W.J., Plafker, G., Wilson, F.H., 1994. Geology of south-central Alaska. In: Plafker, G., Berg, H. (Eds.), The Geology of North America. In: The Geology of Alaska, vol. G1. Geological Society of America, Boulder, CO, pp. 311–366.
- Page, R., Biswas, N., Lahr, J., Pulpan, H., 1991. Seismicity of continental Alaska. In: Neotectonics of North America, vol. 1, pp. 47–68.
- Page, R.A., Stephens, C.D., Lahr, J.C., 1989. Seismicity of the Wrangell and Aleutian Wadati–Benioff zones and the North American plate along the Trans-Alaska Crustal Transect, Chugach Mountains and Copper River basin, southern Alaska. *J. Geophys. Res.* 94 (B11), 16059–16082.
- Parsons, B., Sclater, J.G., 1977. An analysis of the variation of ocean floor bathymetry and heat flow with age. *J. Geophys. Res.* 82 (5).
- Plafker, G., Gilpin, L.M., Lahr, J.C., 1994a. Plate 12: Neotectonic map of Alaska. In: Plafker, G., Berg, H. (Eds.), The Geology of North America. In: The Geology of Alaska, vol. G1. Geological Society of America, Boulder, CO.
- Plafker, G., Moore, J.C., Winkler, G.R., 1994b. Geology of the southern Alaska margin. In: Plafker, G., Berg, H. (Eds.), The Geology of North America. In: The Geology of Alaska, vol. G1. Geological Society of America, Boulder, CO, pp. 389–449.
- Preece, S.J., Hart, W.K., 2004. Geochemical variations in the < 5 Ma Wrangell volcanic field, Alaska: Implications for the magmatic and tectonic development of a complex continental arc system. *Tectonophysics* 392, 165–191.
- Qi, C., Zhao, D., Chen, Y., 2007. Search for deep slab segments under Alaska. *Phys. Earth Planet. Inter.* 165, 68–82.
- Ratchkovski, N.A., Hansen, R.A., 2002. New evidence for segmentation of the Alaska subduction zone. *Bull. Seismol. Soc. Amer.* 92 (5), 1754–1765.
- Redfield, T.F., Scholl, D.W., Fitzgerald, P.G., Beck, J.M.E., 2007. Escape tectonics and the extrusion of Alaska: Past, present, and future. *Geology* 35 (11), 1039–1042.
- Ridgway, K., Thoms, E., Layer, P., Lesh, M., White, J., Smith, S., 2007. Neogene transpressional foreland basin development on the north side of the central Alaska Range, Usibelli Group and Nenana Gravel, Tanana basin. *Spec. Pap., Geol. Soc. Am.* 431, pp. 507–547.
- Sato, T., Larsen, C.F., Miura, S., Ohta, Y., Fujimoto, H., Sun, W., Motyka, R.J., Freymueller, J.T., 2011. Reevaluation of the viscoelastic and elastic responses to the past and present-day ice changes in southeast Alaska. *Tectonophysics* 511 (3), 79–88.
- Savage, J., 1983. A dislocation model of strain accumulation and release at a subduction zone. In: Solid Earth (1978–2012). *J. Geophys. Res.* 88 (B6), 4984–4996.
- Schellart, W.P., Stegman, D.R., Freeman, J., 2008. Global trench migration velocities and slab migration induced upper mantle volume fluxes: Constraints to find an earth reference frame based on minimizing viscous dissipation. *Earth-Sci. Rev.* 88, 118–144.
- Schultz, R.A., Aydin, A., 1990. Formation of interior basins associated with curved faults in Alaska. *Tectonics* 9 (6), 1387–1407.
- Smith, W.H.F., Sandwell, D.T., 1997. Global sea floor topography from satellite altimetry and ship depth soundings. *Science* 277, 1956–1962.
- Song, T.A., Simons, M., 2003. Large trench-parallel gravity variations predict seismogenic behavior in subduction zones. *Science* 301, 630–633.
- Spotila, J.A., Buscher, J.T., Meigs, A.J., Reiners, P.W., 2004. Long-term glacial erosion of active mountain belts: Example of the Chugach–St. Elias Range. *Geology* 32 (6), 501–504.
- Stephens, C.D., Fogelman, K.A., Lahr, J.C., Page, R.A., 1984. Wrangell Benioff zone, southern Alaska. *Geology* 12, 373–376.
- Stout, J.H., Chase, C.G., 1980. Plate kinematics of the Denali fault system. *Can. J. Earth Sci.* 17, 1527–1537.
- Syracuse, E.M., Abers, G.A., 2006. Global compilation of variations in slab depth beneath arc volcanoes and implications. *Geochem. Geophys. Geosyst.* 7 (5), Q05017.
- Thatcher, W., 2009. How the continents deform: The evidence from tectonic geodesy. *Annu. Rev. Earth Planet. Sci.* 37, 237–262.
- Triplehorn, D.M., Drake, J., Layer, P.W., 2000. Preliminary $^{40}\text{Ar}/^{39}\text{Ar}$ ages from two units in the Usibelli Group, Healy, Alaska: New light on some old problems. In: Pinney, D.S., Davis, P.K. (Eds.), Short Notes on Alaska Geology 1999: Professional Report 1191. Alaska Division of Geological & Geophysical Surveys, pp. 117–127.
- Turcotte, D.L., Schubert, G., 2002. *Geodynamics*, 2nd edition. Cambridge University Press.
- Wahrhaftig, C., 1987. The Cenozoic section at Suntrana, Alaska. In: Hill, M. (Ed.), Geological Society of America, Cordilleran Section, Centennial Field Guide. Geological Society of America, pp. 445–450.
- Weidner, D., Chen, J., Xu, Y., Wu, Y., Vaughan, M., Li, L., 2001. Subduction zone rheology. *Phys. Earth Planet. Inter.* 127 (1–4), 67–81.
- Wessel, P., Smith, W.H.F., 1991. Free software helps map and display data. *EOS Trans. AGU* 72 (41), 441–446.
- Wolf, L., Stone, D.B., Davies, J.N., 1991. Crustal structure of the active margin, south central Alaska: An interpretation of seismic refraction data from the Trans-Alaska Crustal Transect. *J. Geophys. Res. B* 10, 16455–16469.
- Yin, A., Rumelhart, P., Butler, R., Cowgill, E., Harrison, T., Foster, D., Ingersoll, R., Qing, Z., Xian-Qiang, Z., Xiao-Feng, W., et al., 2002. Tectonic history of the Altyn Tagh fault system in northern Tibet inferred from Cenozoic sedimentation. *Geol. Soc. Am. Bull.* 114 (10), 1257–1295.
- Zhao, D., Christensen, D., Pulpan, H., 1995. Tomographic imaging of the Alaska subduction zone. *J. Geophys. Res.* 100 (B4), 6487–6504.
- Zhong, S., 2006. Constraints on thermochemical convection of the mantle from plume heat flux, plume excess temperature, and upper mantle temperature. *J. Geophys. Res.* 111, B04409.
- Zhong, S., Gurnis, M., Moresi, L., 1998. Role of faults, nonlinear-rheology, and viscosity structure in generating plates from instantaneous mantle flow models. *J. Geophys. Res.* 103 (B7), 15255–15268.